WIND MEASUREMENTS IN A SQUARE PLOT ENCLOSED BY A SHELTER FENCE

JOHN D. WILSON and THOMAS K. FLESCH
Department of Earth and Atmospheric Sciences, University of Alberta, Edmonton, Canada

(Received in final form 16 January 2003)

Abstract. Wind statistics were measured within a square plot (sidelength $D = 20$ m) that was sheltered on all four sides by a porous plastic windbreak fence (height $h = 1.25$ m, resistance coefficient $k_{r0} = 2.4$, porosity $p = 0.45$), standing on otherwise uniform land (sparse stubble, roughness length $z_0 \approx 0.015$ m). At any given point within the plot, short term wind statistics were extremely sensitive to the mean wind direction relative to the fences. Whereas the entire plot was sheltered from a wind blowing normal to any side of the plot, whenever the wind was oriented so as to blow over a *corner*, wind reduction was observed only over a small fraction of the plot, in the near lee of the upwind fences.

Keywords: Corner effect, Shelter, Vortices, Wind, Windbreak.

1. Introduction

Networks of intersecting windbreaks are intended to provide shelter against strong winds incident from several quarters, and may be seen, for example, in New Zealand kiwi fruit orchards. However it has long been known (e.g., Richards et al., 1984; Richards, 1986) that areas lying downwind from windbreak *corners* receive little or no protection, due to enhanced downward momentum transport by a vortex pair shed from the corner.

Here we report wind measurements in an isolated square plot surrounded by a porous shelter fence, on otherwise open land (Figure 1). While these data may be indicative of the situation in more complex windbreak networks, our main purpose is to encourage further assessment of whether present wind models, either based on the Reynolds-averaged Navier–Stokes (RANS) equations or on large-eddy simulation (LES), are competent to describe this type of flow (Wilson and Yee, 2003). Strong pressure gradients, inhomogeneity on all three spatial axes, and the generation of large vortices interacting with those naturally occurring in the surface layer, render the windbreak array a challenging problem for computational fluid mechanics.

A complication in the practical application of windbreak arrays is that a bluff body like a windbreak casts a turbulent wake, so that the staggering of windbreaks places the allegedly protected downwind region in a zone of increased turbulence. According to Judd et al. (1996), the upstream members of an array of windbreaks

Boundary-Layer Meteorology **109:** 191–224, 2003.

Figure 1. Windbreak experiment, Ellerslie, Alberta. A view to the south-west, showing several of the seven cup anemometers in-plot, a three-dimensional sonic, and a pvc manifold on ground (from which methane was released during gas dispersion trials described elsewhere).

may be considered as 'an additional upstream roughness' having two main consequences: 'an overall decrease in wind-speed ... due to upwind (windbreaks)'; and, 'an increase in ambient turbulence leading to a decrease in the shelter efficiency of any one break in a multiple array relative to an equivalent single break'. Judd et al. (1996) concluded that the 'non-local' shelter afforded by an array as a whole dominates the reduced effectiveness of any *one* of its members due to enhanced turbulence (which causes faster recovery of the velocity in the wake of any *one* member of the array), observing 'windspeeds within a multiple array that are smaller than those behind a single windbreak, given identical external conditions'.

As we shall show, the situation is even more complex for networks of intersecting windbreaks. In the next section we review the aerodynamics of wind through barriers, with an emphasis on the form of the governing equations and the insight that is easily gained from them (without necessity to solve them). Readers whose interest lies with the experimental data may wish to proceed directly to the details and results of our experiment.

2. Overview of the Aerodynamics of a Porous Windbreak

Wind drag on a porous screen, mesh or fence is naturally characterized in terms of a dimensionless 'resistance coefficient', k_r (Laws and Livesey, 1978), which is defined in relation to the pressure drop across the material in a reference flow. A sheet of the given material is mounted with its normal inclined at angle α away from the upwind streamlines, and blocks the passage of a confined, uniform (shearless, laminar) stream of fluid. The resistance coefficient of the material is defined by

$$p_1 - p_2 = k_r(\alpha)\rho V^2 = k_{r0}\rho(V\cos\alpha)^2, \tag{1}$$

where $p_1 - p_2$ is the bulk pressure drop across the barrier (measured away from the immediate region of the mesh), ρ is the fluid density and V is the *speed* of the upwind stream. Thus

$$k_r(\alpha) = k_{r0}\cos^2\alpha, \tag{2}$$

where k_r is the resistance coefficient for an arbitrary inclination of the barrier, and the additional subscript on k_{r0} signifies the value in the case that the flow is normal to the screen. For most windbreak constructions, k_{r0} is insensitive to wind speed and in consequence velocity ratios are universal; but a variation of k_{r0} with a Reynolds number based on mesh diameter may be seen with some types of windbreak fabric.

In the case that the windbreak is composed of trees or bushes, the natural aerodynamic description is in terms of the local plant area density A [m^2 m^{-3}] and the local drag coefficient of plant parts C_d, both of which may vary in all three directions (x, y, z).

2.1. Case of a wind normally-incident on a long, isolated fence

The effects of a long, straight, isolated, porous fence on a neutrally-stratified wind blowing approximately normal to the fence are well known (Raine and Stevenson, 1977; McNaughton, 1988, 1989), and in this simplest of windbreak flows the most important governing dimensionless parameters are $(h/z_0, k_{r0})$. In the near lee of the fence, at heights $z \lesssim h$, a reduction in mean windspeed is observed, with the minimum mean speed occurring at a downwind distance of about $x/h \approx 3 - 5$, and with a recovery beyond that point.* Qualitatively, this is just the behaviour one would anticipate from the mean streamwise momentum equation,

$$\begin{aligned}\frac{\partial}{\partial x}\left(\overline{u}^2 + \overline{u'^2} + \overline{p}\right) + \frac{\partial}{\partial z}\left(\overline{u}\,\overline{w} + \overline{u'w'}\right) \\ = -k_{r0}\overline{u}\sqrt{\overline{u}^2 + \overline{w}^2}\quad \delta(x-0)s(z-h)\end{aligned} \tag{3}$$

* The factors affecting the location of the minimum windspeed behind a windbreak have been studied numerically by Wang and Takle (1997).

and the applicable boundary conditions.* Equation (3) is driven out of equilibrium ($\overline{u} = \overline{u}_0(z)$; $\overline{w} = \overline{p} = 0$) by the momentum sink at the fence, i.e., the term on the r.h.s., in which $s(z-h)$ is a dimensionless step function (unity for $z \leq h$ and zero for $z > h$) and the delta-function specifies the alongwind location of the fence. The disturbance in mean kinematic pressure $\overline{p}$, generated by the interaction of the wind with the barrier, results in an adverse pressure gradient ($\partial\overline{p}/\partial x \geq 0$) both upwind and downwind of the barrier (for observations, see Wilson, 1997).

According to Wilson et al. (1990) the fractional wind reduction at the location of minimum velocity is approximately**

$$\frac{\Delta U}{U_0} \equiv \frac{U_0(z) - U(x,z)}{U_0(z)} = \frac{k_{r0}}{(1+2k_{r0})^{0.8}}. \tag{4}$$

For the plastic windbreak of the present study, for which $k_{r0} = 2.4$, Equation (4) would imply that the minimum relative windspeed to be expected (in neutral flow perpendicular to a long section of this fence, in isolation) is $U/U_0 = 0.41$, occurring somewhere around $x/h \approx 4$. As will be seen, the minimum windspeed actually observed in the plot (*enclosed* by the windbreak) was slightly lower.

Deceleration of the near-ground wind ($z < h$) near the fence necessitates a speed-up zone (jet) over the top of the fence, and the junction of these two regions (low speed wake; jet aloft) implies a zone of strong mean wind shear, which results in a turbulent wake spreading downwind from $x \sim 0$, $z \sim h$ and touching ground at roughly $x/h = 8-10$. Beneath this wake region is a 'quiet zone', i.e., a ground-based, protected region near the fence, within which not only mean windspeeds, but also the turbulent velocity variances, are reduced (Raine and Stevenson, 1977; Wilson, 1987). The factors influencing the turbulence around a windbreak can be detected in the Reynolds equation for streamwise velocity variance $\overline{u'^2}$ ($\equiv \sigma_u^2$),

$$\begin{aligned}
\frac{\partial}{\partial x}\left(\overline{u}\,\overline{u'^2} + \overline{u'^3}\right) \; + \; & \frac{\partial}{\partial z}\left(\overline{w}\,\overline{u'^2} + \overline{w'u'^2}\right) \\
&= -2\overline{u'^2}\,\frac{\partial \overline{u}}{\partial x} - 2\,\overline{u'\,w'}\,\frac{\partial \overline{u}}{\partial z} \\
&- \; R_{xx} + PT_{xx} - \epsilon_{xx} \\
&- \; 4\,k_r\,|\overline{u}|\,\overline{u'^2}\,\delta(x-0)s(z-h).
\end{aligned} \tag{5}$$

In Equation (5), R_{xx} represents the redistribution term (which tends to equalize σ_u, σ_v and σ_w), PT_{xx} represents the pressure transport term, and ϵ_{xx} is viscous

* In Equations (3) and (5), $\overline{u}$ is the streamwise mean velocity component; we use the symbol U to denote mean cup windspeed, $U = \overline{\sqrt{u^2+v^2}}$.

** The distinction between $\overline{u}$ and U can here be dropped. The formula stems from numerical experiments (Wilson, 1985) using a wind model that had been proven to be in good agreement with the field experiment of Bradley and Mulhearn (1983).

dissipation. Shear production ($-\overline{u'w'}\ \partial\overline{u}/\partial z$) accounts for the turbulent wake of a windbreak. The final term in Equation (5), a variance sink due to the interaction of the flow with the fence, was derived heuristically by Wilson (1988), and from the computational perspective is the 'cause' of the 'quiet zone'.

2.2. Barriers set obliquely to the flow

The situation when the mean wind blows at oblique incidence towards a long, straight, isolated windbreak has received less study. Mulhearn and Bradley (1977) carried out a wind-tunnel study of the flow of a simulated neutral atmospheric surface layer through a finite, oblique, porous fence. They noted the following pattern of the airflow far from the ends of the barrier (note: bracketed phrases in italics have been added by the present authors): 'Upwind of the fence, the air close to the ground is deflected along the shelterbelt (*'reluctant' to pass through; i.e.,* $\partial\overline{p}/\partial x_n$, *the component of the pressure gradient normal to the fence, is adverse, upwind from the fence*). As the air passes through the barrier (*compelled by the 'favourable' cross-barrier pressure gradient*), it is deflected back to be more nearly perpendicular to the fence and is accelerated. Then in the region 1.5 to 7 fence-heights downwind, the air close to the surface slows down abruptly and is deflected towards a line parallel to the barrier once again (*dominated by the along-fence pressure gradient?*), before tending back to the ambient flow direction further downstream (*a return to the equilibrium conditions for the given flow*)'. They concluded that 'the flow close to the surface downwind of a shelterbelt is very sensitive to the orientation of the barrier with respect to the wind'.

Seginer (1975) measured mean windspeeds downwind from a porous fence composed of plywood strips. Taking the x-axis normal to the windbreak, Seginer's observations indicate that, with increasing obliquity of the approach flow, the location x_{min} of minimum mean windspeed moves to smaller x/h (i.e., closer to the windbreak) while the relative windspeed $U(x_{\min}, z_m)/U_0(z_m)$ at this most sheltered point systematically increases (inferior wind reduction in oblique flow). The 'protected distance' (range over which the relative windspeed falls below 0.8) also decreased with increasing obliquity of the approach flow (a summary of these and other observations of 'protected distance' is given by Heisler and Dewalle, 1988). These trends, also noted by Richards et al. (1984) on the basis of wind-tunnel simulations, have been replicated in numerical simulations by Wang and Takle (1996), the modelling results showing that the location $x_{\min}/h$ of best mean wind reduction and the relative windspeed at that point both depend on observation height and windbreak structure. In part the reduced effectiveness of a protecting fence in oblique winds owes to the fact that a given point, lying at a fixed distance x along the normal to the fence, lies *further* from the part of the fence protecting it, as obliquity increases; however, as indicated by Equation (2), for a given fixed approach *speed*, the back-pressure of the fence on the flow drops rapidly with increasing obliquity.

It has already been mentioned that mean winds *above* a porous windbreak are increased, due to the upward displacement of mean streamlines by the barrier. However, in their measurements of mean cup windspeed about a thin porous fence composed of wooden slats, Jacobs and Wartena (1987) found that in oblique flow a region of *increased* mean windspeed occurred in the lee of the barrier, moving closer to the barrier with increasing obliquity (e.g., mean windspeed increased for all $z/h \leq 5$ at $x/h = 10-15$, when the approach wind direction is 40° away from the normal to the fence). Jacobs and Wartena termed this 'overshoot', and attributed it qualitatively to bending (by differential advection) of initially-straight transverse vortices, implicit in the shear of the approach wind, upon their encounter with the ends of the (finite) fence. They also noted that the pattern of the speed fluctuations was affected by flow obliquity, for example at $z/h = 0.3$, low enough that in normally-incident winds one would expect to observe a 'quiet zone' of reduced turbulence out to about $x/h \approx 5-8$, increasing obliquity beyond about 30^o greatly shortened the x-wise span of the quiet zone.

2.3. Flow around barriers with corners

Koo and James (1973) measured the flow that results in the lee of a *kinked* porous screen partially blocking a uniform, confined, laminar stream. Along the centreline in the lee of a 90° kink (flow symmetrically incident on a right-angle corner) they observed virtually no reduction in velocity, while as the corner angle was widened to 120° a velocity deficit was measured in the wake along the centreline. Koo and James considered these effects to be consistent with their (non-linear, but two-dimensional) vorticity-conservation theory, which however is obviously not applicable to a finite barrier in the atmosphere.

Richards et al. (1984), reporting on wind-tunnel experiments with a porous fence in a wall shear layer, may have been the first to systematically study the mean wind pattern within a rectangular windbreak. They noted a dramatic sensitivity to upstream wind direction, with very poor protection of 'sheltered' areas lying downwind from windbreak corners, and considered this corner effect as 'responsible for most of the wind damage (in some New Zealand orchards)'. According to Richards (1986), paired streamwise vortices, shed off the sharp corner, cooperate to create a strong downdraft along the diagonal of the plot, and cause the rapid recovery in mean wind speed.

3. Details of Windbreak Experiment

The experiment took place from 23 May to 12 June, 2001 at the University of Alberta farm at Ellerslie, Alberta, in a large, even field of sparse stubble (surface roughness length $z_0 \approx 0.015$ m). The overall slope of the land was less than about 1–2%, and for the range of absolute wind directions whence the present data derive,

the fetch of uniform conditions upstream from the site ranged from a minimum* of about 200 m in south winds, up to about 400 m in west winds; an isolated tree about 300 m distant to the south–west ought to have had little influence on our observations.

A porous plastic windbreak fence** (height $h = 1.25$ m, resistance coefficient $k_{r0} = 2.4$, porosity $p = 0.45$) was erected in a square of sidelength $D = 20$ m ($D/h = 16$). This configuration (see Figure 1) was equivalent, except as regards surface roughness length, to that studied earlier by Argete and Wilson (1989), who had focused on the disturbance to equivalent temperature within the plot.

3.1. Instruments and their positions

A 6 m tower outside the plot (standing $10.4h$ west and $0.8h$ south of the south-west corner of the fence) was instrumented with cup anemometers (Climet model 011-4) at heights z = (0.65, 1.12, 2.12, 3.6, 6.05) m; two shielded and ventilated thermocouple pairs measuring temperatures differences over spans z = (0.29–1.35) m and z = (1.35–5.75) m; a wind vane at z = 1.73 m; and (on most occasions) a Campbell Scientific (CSI) *CSAT*3 three-dimensional sonic anemometer at a height near $z = 2$ m. Orientation of the sonic was adjusted to ensure good exposure, but during unattended measurements changes in wind direction sometimes implied a wind from the back of the instrument (appropriate attention to this was paid during the analysis).

Seven more cup anemometers (Climet 011-4) and a second *CSAT*3 were exposed inside the plot, the cups being always at height $z/h = 0.5$, i.e., $z = 0.63$ m, the same height as the lowest anemometer on the reference tower. Letting ($x = y = 0$) define a coordinate origin at the centre of the plot, and ($x/h = -8$, $y/h = 8$) its north-west corner (etc.), we placed the in-plot anemometers as follows:

Configuration A: anemometers at plot centre (0, 0); plot 'sides', west (−4, 0), and east (+4, 0); plot 'corners', north-west (−4, +4), north-east (+4, +4), south-east (+4, −4), and south-west (−4, −4). In this configuration distance to the nearest fence was $4h$ for all but centre anemometer. According to Equation (4), if we ignored the geometric complexity of the plot, we might expect that anemometers at about $4h$ from a fence would report a windspeed diminished to only about 40% of the open windspeed.

Configuration B: anemometers at plot centre (0, 0); plot 'sides', west (−6, 0), and east (+6, 0); plot 'corners', north-west (−6, +6), north-east (+6, +6), south-east (+6, −6), and south-west (−6, −6).

A datalogger (Campbell Scientific CR7) recorded 15-minute averages of the cup windspeeds, the temperature differences, and the (vane) wind direction, while a

* The fetch interruption was an ordinary wire stock fence, and the surface further upstream would have had a roughness length very similar to that of our experimental field.

** Tensar Corporation.

second logger (Campbell Scientific CR10X) recorded simultaneous wind statistics from the two sonics (all first- and second-moments).

4. Data Processing

Data were recorded semi-continuously over a 20-day interval. Over several of those days, the instruments operated unattended, and it was especially critical not to be misled by including contaminated measurements, such as might stem from periods when the cups on the tower were in the wake of the tower itself, or of the fences. Furthermore, in any period during which a sonic was oriented such that the mean wind approached the instrument from the rear, it is appropriate to view turbulence statistics from that instrument with some reservation.

Valid periods for the analysis were selected according to the following criteria: (a) all mean cup windspeeds must exceed 1 m s^{-1} (thereby we hope to have eliminated periods of threshold errors, i.e., cup stoppages); (b) mean wind direction from the vane was regarded as invalid if it lay in the range $\pm 30°$ relative to north, to eliminate error due to the dead band of the potentiometer (a north wind would have placed the vane in the dead band, whose width was about $\pm 5°$); (c) mean wind directions from vane and tower sonic* were required to be consistent to within 10° or better, if there was no reason *a priori* to distrust either instrument; (d) a mean wind from the back of a sonic was not considered cause to reject the sonic estimate of mean wind direction, however sonic estimates of turbulence during such intervals were considered invalid; (e) unless otherwise noted, data were rejected unless $160° \leq \beta \leq 330°$, to ensure the tower was never in the wake of the fence, nor were the cups on the tower in the wake of the tower.

In results to follow, 'mode α' signifies that all these criteria were met; data satisfying a less-stringent condition $135° \leq \beta \leq 350°$ on wind direction, are sometimes displayed (with distinguishable symbols). We did not exclude runs occurring around times of transition in stratification.

The sonic on the tower is of course presumed to see undisturbed flow. Accordingly for each averaging interval, velocity statistics from the tower-sonic were transformed** by a sequence of two coordinate rotations (Kaimal and Finnigan, 1994), setting first $\overline{v} = 0$ (yaw correction), then $\overline{w} = 0$ (pitch correction).

* Sonic mean wind direction was computed as $\arctan(\overline{v}/\overline{u}) + \beta_0$, where $\overline{u}, \overline{v}$ are pre-rotation and relative to the frame of the sonic, and where β_0 rotates from the sonic frame (which was frequently adjusted to optimize exposure of the instrument to prevailing winds) to a geographic N–S/E–W frame.

** Run-by-run coordinate rotations were chosen because the orientation of the sonic was adjusted frequently throughout the experiment, a step which prohibits the definition of a tilt correction based solely on apparent mean vertical velocity W versus absolute wind direction.

4.1. ADJUSTMENT OF CUP ANEMOMETERS FOR OVERSPEEDING

Cup anemometers are subject to several types of errors (see Papadopoulos et al., 2001, and earlier studies they cite). By selecting only runs with all speeds exceeding 1 m s^{-1}] we presume we have eliminated most (if not all) periods when cups might have intermittently stalled (threshold errors). However our cup anemometers would have been subject to 'overspeeding' errors, i.e., an asymmetry in the acceleration/deceleration response to gusts in the horizontal plane, as well as to 'tilt errors', which are implied by the failure of a cup anemometer to respond to the wind vector in proportion to the cosine of its elevation angle relative to the plane of cup rotation. Both of these types of error would potentially be increasingly serious in the wake of the shelter fences, where (as will be shown) the mean flow was not horizontal.

Many periods of record were available for which mean cup windspeeds on the tower could be interpolated to the height of the sonic anemometer (according to the best-fit Monin–Obukhov profile), and compared with the (effective) cup windspeed $U_s = \overline{\sqrt{u^2 + v^2}}$ reported by the sonic over the same interval. The fractional error $\Delta = (U - U_s)/U_s$ showed no systematic relationship with turbulence intensity ($i_k = \sqrt{k}/U_s$, where k is the turbulent kinetic energy) or sonic mean vertical velocity $\overline{w}/U_s$, therefore we simply adjusted all cup windspeeds by the multiplicative factor $f_{os} = 1/1.08$. Observations from a sonic temporarily replacing the cup anemometer at plot centre (Figure 7, discussed in Section 5.1) provide confirmation that the cup anemometers measured the mean value of $\sqrt{u^2 + v^2}$ adequately, even within the disturbed flow.

4.2. SELF-CONSISTENCY OF THE TWO SONIC ANEMOMETERS

After completion of the shelter experiments, the in-plot sonic was mounted alongside the tower sonic, the two facing west at $z = 2$ m and separated by ≈ 0.6 m laterally along an axis lying approximately south-west to north-east (the separation was thus oriented to minimize flow interference between the sonics, during the generally north-west winds of that afternoon). We recorded time series at 10 Hz from the two sonics, from which we computed statistics *rejecting* samples for which instantaneous wind direction did not lie in the optimal window $-45° \leq \beta_{\text{frame}} \leq 65°$. Post-rotation $\sigma_{u,v,w}$ were consistent to 3% or better, while estimates of $\sqrt{-\overline{u'w'}}$ were consistent to within 10% or better.

4.3. SURFACE-LAYER SCALING PARAMETERS OF THE APPROACH FLOW

Following application of the overspeeding correction, theoretical mean wind and temperature profiles were fitted to the observed profiles $U_0(z)$, $T_0(z) - T_{\text{ref}}$ on the tower, so as to determine the surface-layer parameters, by assuming Monin–Obukhov (MO) similarity applies. We used the best least squares procedure

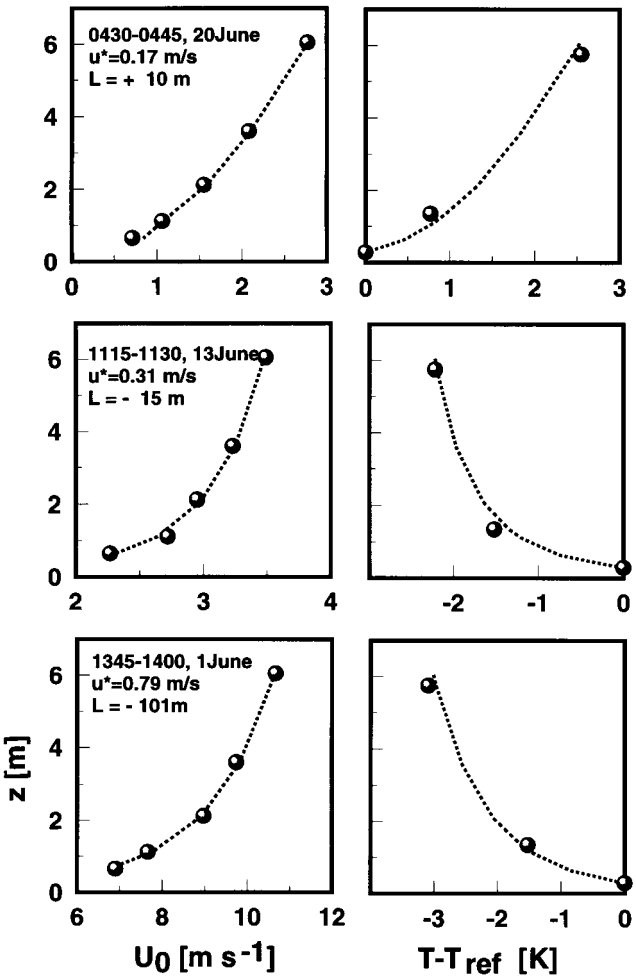

Figure 2. Vertical profiles of mean cup windspeed (adjusted by factor 1.08 for overspeeding) and mean temperature difference relative to the lowest thermocouple junction; ●, observations; lines, the best-fit Monin–Obukhov profile.

described by Argete and Wilson (1989) to determine u_*, T_*; as earlier, for unstable stratification we used the MO functions recommended by Dyer and Bradley (1982), and for stable stratification we used those of Webb (1970). Resolution of the search procedure was $\triangle u_* = 0.01$ m s^{-1}, $\triangle T_* = 0.02$ K (we presupposed the von Karman constant $k_v = 0.4$). The tower measurements supplied us with the surface-layer state as denoted (u_{*t}, L_t, β_t, z_0). Figure 2 gives examples of measured (and fitted MO) profiles from the tower.

4.4. SYMMETRY

The mean wind (or any other statistic) in the plot must be regarded as having a functional dependency at least as complex as:

$$\frac{U}{u_{*0}} = F\left(\frac{x}{h}, \frac{y}{h}, \frac{z}{h}, \frac{D}{h}, \frac{h}{z_0}, k_{r0}, \beta, \frac{\delta}{h}, \frac{u_{*0}h}{\nu}\right), \tag{6}$$

where the first three arguments specify position, the next three the character of the windbreak, β is mean absolute wind direction, δ is boundary-layer depth, and the final entry is a (large) Reynolds number (intuitively, one would not expect the final two parameters to exert any strong influence on the consequences wrought by the windbreak). The present measurements cover only a narrow region of this parameter space, but we may exploit symmetry of the experimental configuration to make optimal use of what measurements are at hand.

Measurements were made during intervals that covered virtually the full range in absolute mean wind direction $0 \leq \beta \leq 360°$, though as mentioned, we excluded periods that might imply unwanted interactions. Symmetry implies that (to get a complete picture of wind in the whole plot) it would in principle have been sufficient to have placed *all* the instruments in a *single* sector of the plot, e.g., the right-angle triangle whose three sides are defined by the y- (i.e., north–south) axis through plot centre, the northern leg of the fence, and the diagonal $y = x$. However this is not the approach we took, which rather was to place instruments throughout the plot, but at symmetric positions.

Recall that we have defined ($x = y = 0$) as the centre of the plot, and ($x/h = -8$, $y/h = 8$) its north–west corner (etc). For an anemometer at plot centre, a wind direction of $-45°$ (or $45°$) implies the north-west (or north-east) corner lies upstream. It is evident that, by symmetry, one may introduce a 'reduced' mean wind direction β_r spanning $0° \leq \beta_r \leq 45°$ and that a mean wind from any other sector is equivalent to a mean wind direction in this sector. Similarly for 'corner' positions (see the icon on Figure 3) symmetry implies that a complete domain in reduced wind direction is $-45° \leq \beta_r \leq 135°$ ($0°$ being a wind from the 'reduced north'), while for 'side' positions (icon of Figure 5) symmetry implies that $-90° \leq \beta_r \leq 90°$, where $-90°$ is a wind from the 'reduced east.'

It is important to clarify that unless otherwise specified, the term 'reduced mean wind direction' implies a direction derived from wind direction *in the open*, but transformed according to the symmetries in operation at a particular position in the plot.

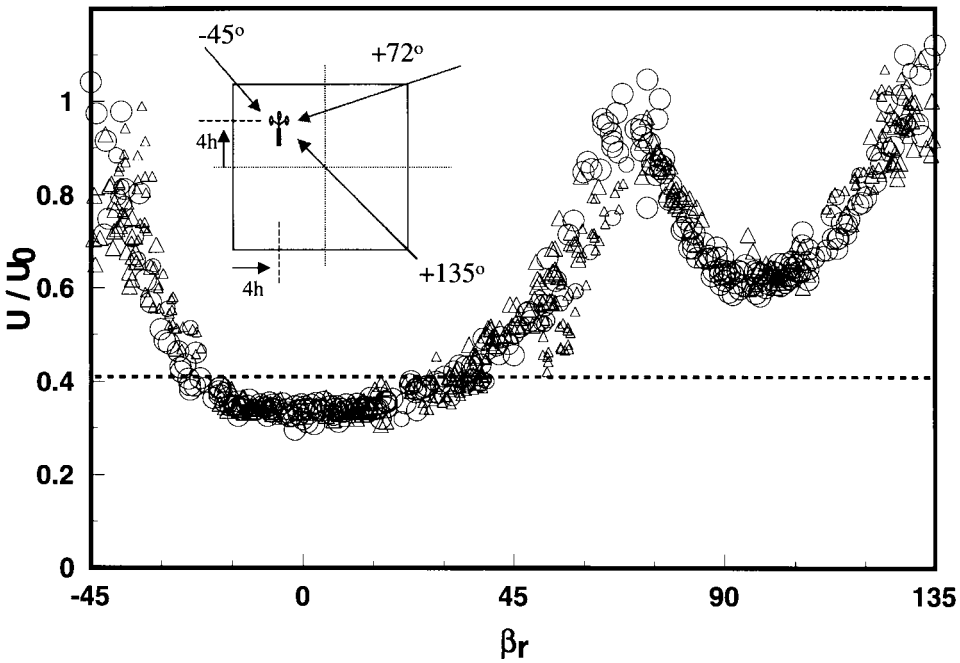

Figure 3. Relative cup windspeed in the square plot, at the corner position $4h$ from fences, as function of reduced mean wind direction for that position (U_0 designates the upstream windspeed at the same height $z/h = 0.5$ as the in-plot anemometers). Corner flow for this position occurs at $\beta_r = (-45°, +72°, +135°)$. ○, Stable stratification; △, unstable stratification. Larger symbols are observations with absolute wind direction in the range $160° \leq \beta \leq 330°$; smaller symbols lie outside this range, but satisfy $135° \leq \beta \leq 350°$. The dashed line (on this and later figures) gives the expected minimum windspeed in the lee of a long straight fence, according to Equation (4).

5. Mean Cup Windspeed in the Shelter

5.1. Angular sensitivity of mean cup windspeed at fixed positions in the plot

Figures 3 and 4 show the observed pattern of reduction in normalized mean cup windspeed in the corner of the plot, as a function of reduced mean wind direction. Speeds have been normalized on U_0, the speed in the open at $z/h = 0.5$, which has been evaluated from the fitted tower profile implied by u_{*t}, L_t, z_{0t}. No overspeeding correction need be applied, since it would in any case cancel in the normalisation.

Regarding the interpretation of Figure 3, recall that an anemometer in this position (the corner of the plot at distance $4h$ from nearest fences) 'sees' corners upwind for (reduced) wind directions $\beta_r = (-45°, 72°, 135°)$, these corners falling at successively increasing upwind distances equal to $(\sqrt{32}, \sqrt{160}, \sqrt{288})h = (5.7, 12.6, 17.0)h$. Evidently there is *no shelter* at an anemometer in the wake

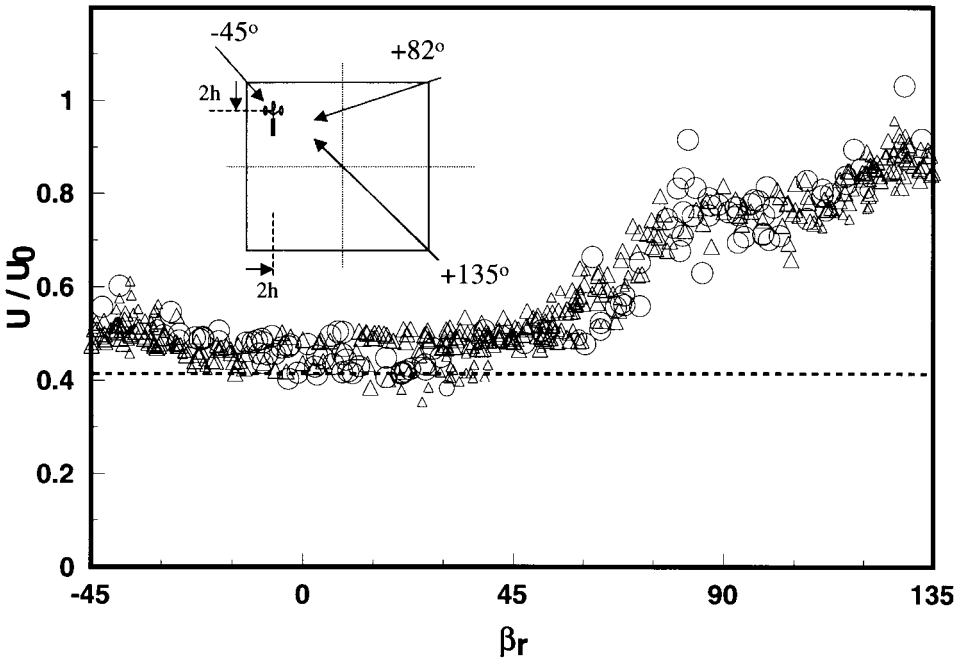

Figure 4. Relative cup windspeed in the square plot, at the corner position $2h$ from fences, as function of reduced mean wind direction. ○, Stable stratification; △, unstable stratification. Larger symbols are observations with absolute wind direction in the range $160° \leq \beta \leq 330°$; smaller symbols lie outside this range, but satisfy $135° \leq \beta \leq 350°$.

of any of these corners, for the reported relative windspeed, rather than having been reduced to as little as only about 41% of the speed in the open, is essentially 100% of the approaching windspeed, if not even slightly *faster* than the approach speed; when the wind blows over a corner, evidently there is some disturbance that enhances downward momentum transport.

In contrast when the wind blows at more-or-less perpendicular incidence ($\beta_r \approx 0°$) over an upwind fence (only $\approx 4h$ distant) and to a corner anemometer, wind reduction is dramatic (relative windspeed $U/U_0 \approx 0.35$) and, surprisingly on first sight, slightly greater than would be expected ($U/U_0 = 0.41$; from Equation (4)) if that upwind segment of fence were infinitely long, and the other fence-sides of the plot were removed. When the wind blows perpendicularly ($\beta_r \approx 90°$) over the 'eastern' (more distant) fence (distance $12h$ upwind), there is a less marked wind reduction (relative windspeed $U/U_0 \approx 0.6$), which (qualitatively) is what one would expect behind a long *isolated* fence, at an observation point this far ($12h$) downwind.* Note also from Figure 3 that the pattern of wind reduction is almost the same under stable stratification as under unstable.

* A computed curve of wind reduction behind an isolated segment of our fence is given on Figure 9.

The anemometer represented by Figure 4 is more tightly wedged into the corner, at a distance of $2h$ from the nearest fences. This close in to the fence, some wind reduction is observed even when the wind blows over the nearby corner ($\beta_r = -45°$). For a wind over the more distant corners ($14.1h$, $19.8h$) at $\beta_r = (82°, 135°)$ a modest wind reduction of order 20% (i.e., $U/U_0 \approx 0.8$) is (usually) seen. Simplifying, in Figure 4 we see a fairly constant level of about 50% wind reduction for wind approach angles lying counter-clockwise of the ('reduced north-east') corner at $\beta_r = 82°$, then an abrupt transition to a more exposed condition ($\approx$ 20% wind reduction; sporadically, and for an unknown reason, sometimes less) for angles clockwise of that corner which imply a longer fetch to the protecting leg of the fence.

Turning now to wind at the 'side position' $(x/h, y/h) = (-4, 0)$, Figure 5 shows three distinct minima in relative windspeed when the wind blows perpendicularly ($\beta_r = -90°, 0°, +90°$) over protecting legs of the fence at progressively larger upstream distances ($4h$, $8h$, $12h$). However when the wind blows over the corners $\beta_r = (-27°, +56°)$ at distances ($8.9h$, $14.4h$) wind reduction by the shelter is erased, and in stable stratification there is indeed a slight *increase* in windspeed in the 'shelter', when the wind passes over the ($\beta_r = +56°$, fetch = $14.4h$) corner. A broadly similar but less strongly modulated angular response occurs at the side position tucked closer in beside a fence at $(x/h, y/h) = (-6, 0)$, as indicated by Figure 6; however in this case there is more than a suggestion that the shelter-erasing capability of (especially) the nearest corner ($\beta_r = -14°$), quite evident in stable stratification, is muted in unstable stratification. The four uppermost ◯ datapoints at $\beta_r \approx -14°$ stem from the east and west anemometers during the late evening of 5 June; wind direction was quite steady ($\sigma_v/U_s \approx 11°$) and aligned with the corner. The nearest comparable corner-flow datapoint under unstable (△) stratification comes from an interval with a considerably more variable wind direction ($\sigma_v/U_s \approx 35°$), and the shelter-erasing corner effect consequently does not show up so markedly as during stable stratification.

In the region $\beta_r = +15 \pm 15°$, Figure 6 indicates two distinct bands (U/U_0 multi-valued at given β_r). From the figure it is evident that this unexpected separation into bands is not explainable as being associated with stability. The data around $\beta_r \approx +15°$ stem from three different days, and broadly cover all times of the day. Each strand is a mix of data from all three days; the upper strand stems mostly (but not entirely) from measurements by the west anemometer, while the lower strand is more evenly a mixture of data from the east and west anemometers (this information is not given on the figure).

Referring back to Equation (6), seven of the nine parameters upon which U/U_0 is anticipated to depend, are *fixed*, at given β_r. The two strands cannot be attributed to an organisation relative to the variability $\sigma_\beta \approx \sigma_v/U_s$ of wind direction. It would be surprising if this band separation hinged on variations in boundary-layer depth δ, but then what other unconsidered parameter could 'split' this curve into two strands? A remote possibility is that variation in the overall windspeed (which im-

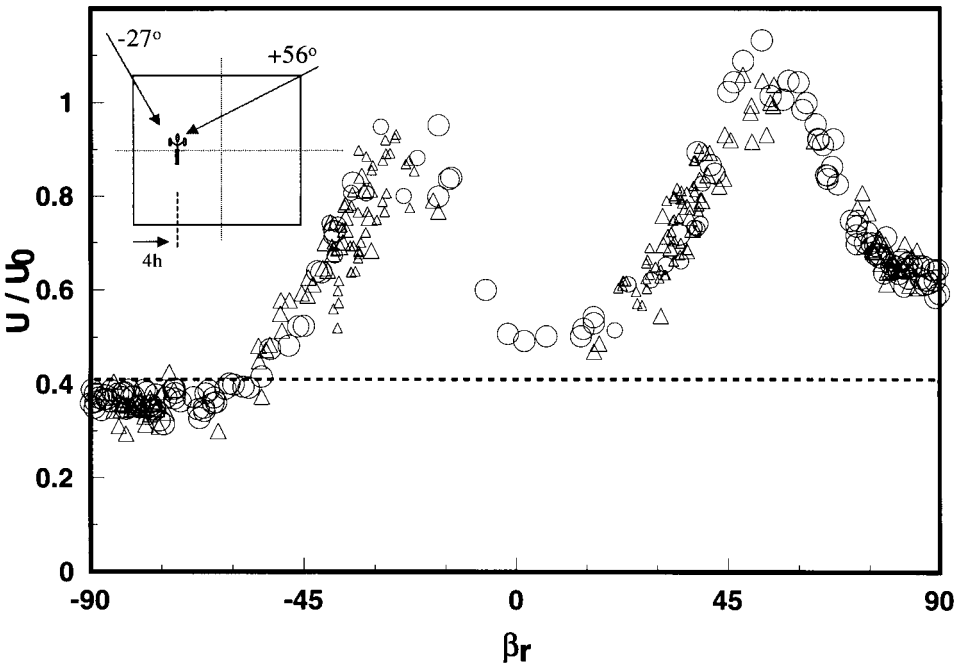

Figure 5. Relative cup windspeed in the square plot, at the side position 4h from the nearest fence, as function of reduced mean wind direction. ○, Stable stratification; △, unstable stratification. Larger symbols are observations with absolute wind direction in the range $160° \leq \beta \leq 330°$; smaller symbols lie outside this range, but satisfy $135° \leq \beta \leq 350°$.

plicitly appears through the Reynolds number in Equation (6)) could have implied bowing of the fence, changing the geometry.

Figure 7 gives the observed wind reduction at the centre of the plot at $z/h = 0.5$, observed both by the cup anemometer, and (during an interval of about two days) by the second sonic (the sonic was placed at plot centre *in lieu of* the cup anemometer, which was removed). In the case of the sonic estimates, it is appropriate to adjust the reference velocity U_0 for height $z/h = 0.5$ (which is derived from the cup anemometers on the tower) for overspeeding: thus, the sonic data plotted on Figure 7 are $\overline{\sqrt{u^2 + v^2}}/(U_0/1.08)$.

There is little less scatter in the sonic-derived estimates of U/U_0 than in the cup estimates, nor do the clouds of sonic and cup data stand apart from one another: the sonic and (adjusted) cup data are, then, in rather good agreement. The data do suggest that wind reduction at plot centre for a wind normal to the fence ($\beta_r = 0°$) is slightly better in stable than in unstable stratification (reduced down-mixing of the wake?), while conversely the poor shelter due to the corner effect when $\beta_r = 45°$ is more marked in stable stratification.

In the case $\beta_r = 0°$, Figure 7 indicates that at the plot centre $U/U_0 \approx 0.5$, i.e., $\approx 50\%$ mean wind reduction, as opposed to the $\approx 60\%$ reduction (according

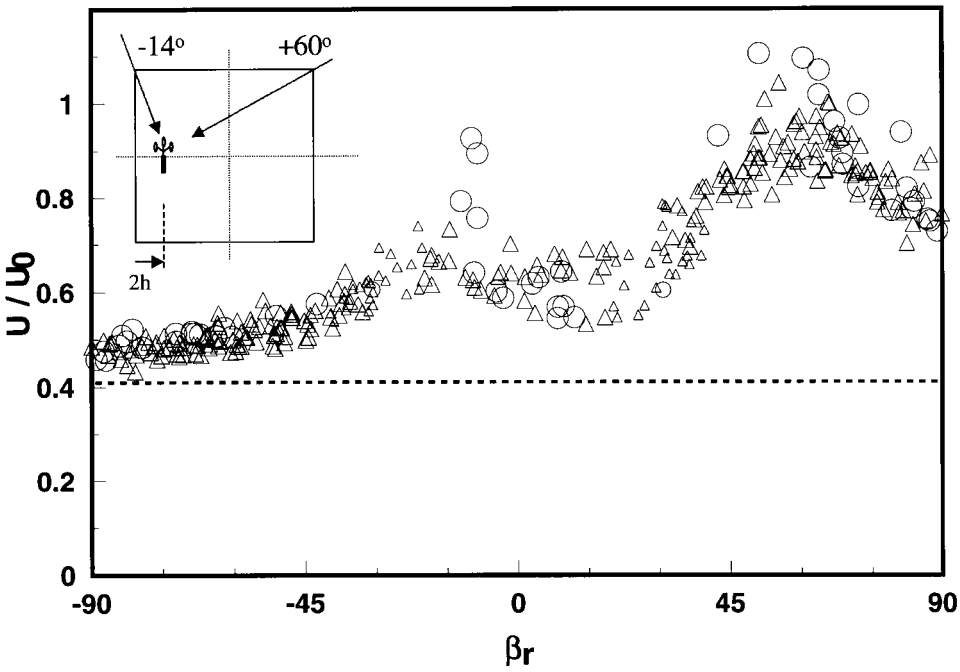

Figure 6. Relative cup windspeed in the square plot, at the side position $2h$ from the nearest fence, as function of reduced mean wind direction. ○, Stable stratification; △, unstable stratification. Larger symbols are observations with absolute wind direction in the range $160° \leq \beta \leq 330°$; smaller symbols lie outside this range, but satisfy $135° \leq \beta \leq 350°$.

to Equation (4)) attainable in the near lee of a long straight section of this fence. Bearing in mind that the plot-centre falls a distance $x/h = 8$ downstream from the fence, i.e., beyond the expected location of minimum windspeed for an isolated fence, one may say that provided $\beta_r \approx 0°$, conditions at plot centre are not very different from what they would be the same distance downwind from an isolated fence: referring ahead to Figure 9, which gives a computed curve of U/U_0 versus x for an isolated fence of this type, we see the computation gives $U/U_0 = 0.47$ for $x/h = 8$.

5.1.1. *Dependence on Averaging Time*

Figure 8 is equivalent to Figure 3, except that it is based on 30-min (rather than 15-min) averages. One might have supposed that an undoubtedly greater standard deviation σ_β of wind direction over the longer averaging interval would 'smear out' the peaks and troughs of the preceding figures. Qualitatively, this is what has happened: notice that, comparing Figures 3 and 8 the high 15-min relative windspeeds ($U/U_0 > 1$) observed in the shelter for corner flows at $\beta_r = -45°$, $+72°$ translate to slightly lower relative windspeeds ($U/U_0 \lesssim 1$) in the 30-min average. But the smoothing effect with increasing averaging time evidently is not

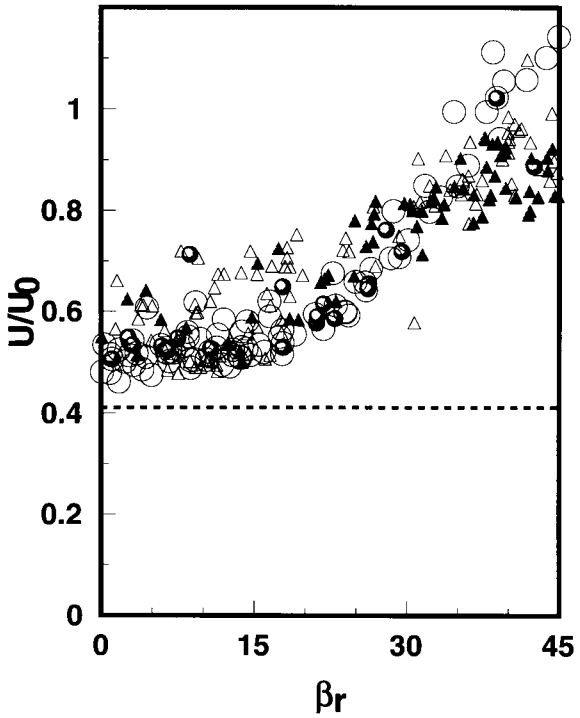

Figure 7. Relative cup windspeed at the centre of the square plot, as function of reduced mean wind direction (note that the horizontal scale has been stretched relative to preceding figures). Observations satisfy $160° \leq \beta \leq 330°$. ○, Stable (open = cup, solid = sonic); △, unstable (open = cup, solid = sonic).

very important, and it was, if anything, even more subtle for the other instrument positions in the shelter.

5.2. Mean cup windspeed in the plot versus effective fetch

At any anemometer in the plot, and for any given mean wind direction (absolute or reduced), there is some well-defined alongwind distance x^* to the nearest upwind fence; e.g., for an anemometer at $(x/h, y/h) = (-4, 4)$ the effective fetch is $x^*/h = (4, 12)$ for reduced wind directions $\beta_r = (0°, 90°)$.

It is straightforward to calculate effective fetch versus β_r; for example at position $(x/h, y/h) = (-4, 0)$ the rule is:

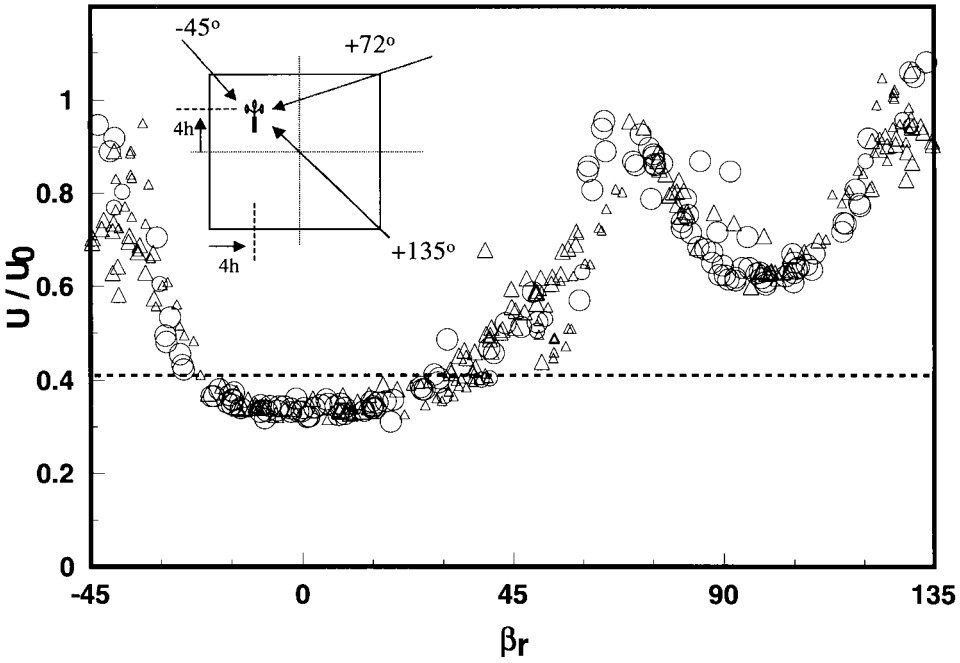

Figure 8. Same as Figure 3, i.e., relative cup windspeed in the square plot, at the corner position $4h$ from fences, except that here the averaging time is 30 min.

$$\begin{aligned}\frac{x^*}{h} &= \frac{4}{\cos(90+\beta_r)}, \quad -90 \leq \beta_r \leq -\text{atan}\left(\frac{4}{8}\right) \\ &= \frac{8}{\cos(\beta_r)}, \quad -\text{atan}\left(\frac{4}{8}\right) \leq \beta_r \leq \text{atan}\left(\frac{12}{8}\right) \\ &= \frac{12}{\sin(\beta_r)}, \quad \text{atan}\left(\frac{12}{8}\right) \leq \beta_r \leq 90.\end{aligned} \tag{7}$$

Figure 9 plots the observed mean (relative) cup windspeed U/U_0 versus effective fetch x^*/h, for all (distinct) positions in the plot that were sampled (centre; two side positions, two corner positions). At any given position, there is a well-defined minimum value for the fetch: $2h$ or $4h$ or (for the anemometer at plot centre) $8h$. Thus on Figure 9 one sees data from a given position in family patterns that slant toward larger U/U_0 in association with larger x^*, corresponding to air passing increasingly more obliquely over a fence.

Also shown on Figure 9 is a RANS computation of the wind reduction expected for neutrally-stratified surface layer flow at perpendicular incidence through an infinitely-long fence (all other parameters matching the present configuration, i.e., $k_{r0} = 2.4$, $h = 1.25$ m, $z_0 = 0.015$ m). The computation is a solution of the conservation equations under the second-order closure of Rao et al. (1974a, b), and follows the methodology of earlier work (Wilson, 1985; Wang and Takle,

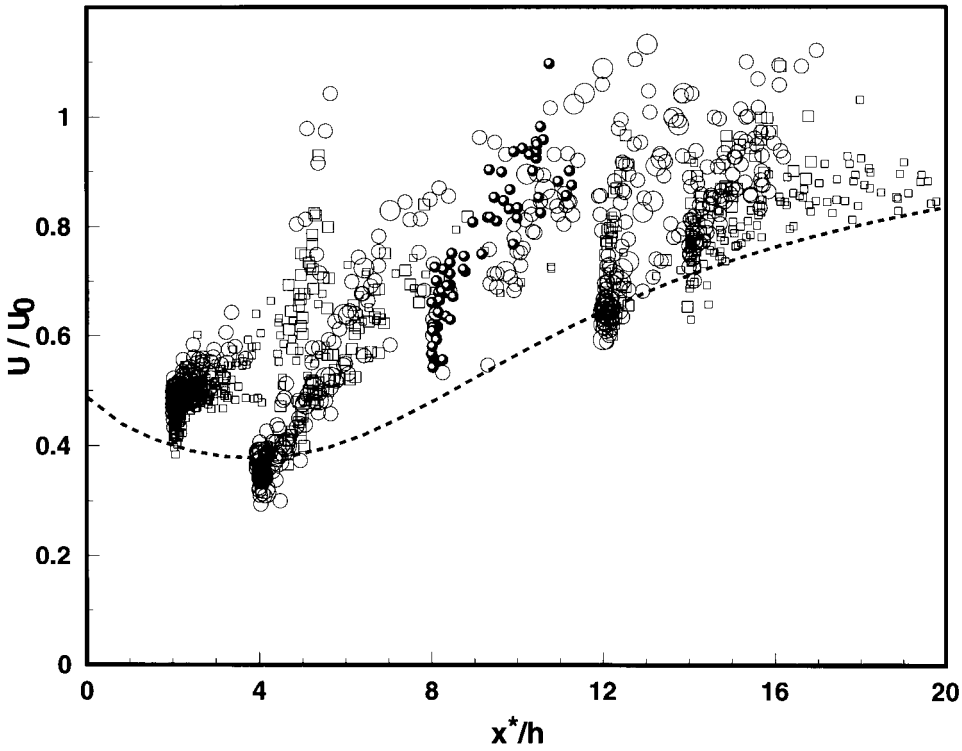

Figure 9. Relative cup windspeed $U(x, z)/U_0(z)$ versus fetch x^* to the nearest upwind fence, for all distinct measurement positions in the square plot: •, plot centre; ○, $4h$ side; ∘, $2h$ side; □, $4h$ corner; ▫, $2h$ corner. Observations satisfy $160° \leq \beta \leq 330°$. The dashed line is a numerical solution for neutrally-stratified flow perpendicular to an infinite fence ($k_{r0} = 2.4$, $h = 1.25$ m, $z_0 = 0.015$ m).

1995; Wilson et al., 2001), which has shown such computations are in good agreement with observations. For the simulation on Figure 9, the computational domain spanned $-10 \leq x \leq 100$ m, $z \leq 50$ m, and gridlengths were $\Delta x = 1$ m, $\Delta z = 0.15$ m ($\Delta x/h = 0.8$, $\Delta z/h = 0.12$).

Evidently the computed solution ('$U^{\mathrm{ref}}(x_*)$') for an isolated fence approximately defines an 'envelope' of best-protection in the more complex winds within our square shelter. The majority of the in-plot windspeeds fall *above* the envelope, indicating a *lessened* effectiveness of the shelter relative to the reference situation, and in these cases the upwind fence lies obliquely across the incident flow, with the highest observed U/U_0 corresponding universally to 'corner flows'. We see a smaller number of values of U/U_0 lying *below* the reference envelope, these corresponding to the circumstance that the wind blew nearly perpendicularly over a side (values of x^*/h very close to 2, 4, 8, 12, 14, the effect being most obvious for $x^*/h = 4, 12$). These occurrences of 'enhanced wind reduction' occurred in both stable and unstable stratification, without evident relation to overall windspeed

or stability, and those at $x^*/h \approx 4$ stem from the $4h$ corner position (Figure 3; $\beta_r = 0°$) and the $4h$ side position (Figure 5; $\beta_r = -90°$).

Can we explain these cases of a slightly more pronounced wind reduction than (on naive first sight) expected? Firstly, we repeat that a reflection-symmetry applies along a straight line through the centre of the plot, in the following circumstances: at the $(2h, 4h)$ side positions when $\beta_r = (-90°, +90°)$; at the $(2h, 4h)$ corner positions when $\beta_r = (-45°, +135°)$; and at plot centre when $\beta_r = (0°, 45°)$. Now let (x', y') be a coordinate system aligned with mean wind direction outside the plot (y' is the crosswind direction). For each of the given cases, the symmetry $\overline{v} = 0$, $\partial()/\partial y' = 0$ prevails along the line through plot centre ($x' = y' = 0$). Thus, along that line, Equation (3) applies ($\overline{u}$ must be interpreted as the component aligned with the mean wind direction outside the plot). Of course this does not mean we have a two-dimensional mean flow: *Only* along this line through plot centre, about which the reflection-symmetry applies, must the terms (in $\overline{v}$ and $\partial/\partial y'$) vanish.

But having identified this (conditional, and localised) simplification of the governing $\overline{u}$ equation, perhaps we can interpret the better mean wind reduction (than the $U/U_0 \approx 0.41$ expected at the equivalent position in perpendicular flow through a long, isolated fence) at the $4h$ corner position ($\beta_r = 0°$) and at the $4h$ side position ($\beta_r = -90°$) as being due to the *nearby imposition of the no-slip condition* $\overline{u} = 0$ along the side-fence only $4h$ distant laterally. Obviously no such (wind-arresting) condition is to be applied when Equation (3) governs (or is solved for) the flow about an isolated fence, and since it is the character of the momentum equations to 'diffuse' the influence of a boundary condition, one may well expect these data of Figure 9 lying *beneath* the wind-reduction envelope of an isolated fence. This explanation also covers the enhanced wind reduction seen on Figure 9 at smaller ($x^*/h \approx 2$) and larger ($x^*/h \approx 12, 14$) downwind distances, and if it is correct, then one must infer that enhanced wind reduction is *not* seen at $x^*/h \approx 8$ because the side fence (along which this no-slip boundary is imposed) is too far away, being in this case distance $\approx 8h$ from the point of observation.

5.3. Contours of Mean Cup Windspeed in the Plot

Owing to symmetry, it suffices to demonstrate the whole field of windspeed in the plot for only the range $0 \leq \beta \leq 45°$ in absolute windspeed, other bands being equivalent. In order that the reader be able to relate the contour plots that follow to the preceding graphs of wind reduction versus *reduced* mean wind direction, Figure 10 gives the reduced mean wind direction at each anemometer position, for absolute wind directions of $\beta = 0°, 15°, 30°, 45°$.

Figures 11 to 14 are hand-drawn* contour plots of wind reduction, for each of these absolute wind directions. The symmetry in the contour patterns for $\beta = 0°$, 45° is mandated, of course, by the assumptions made in the analysis. For wind directions $\beta = 0°, 15°, 30°$, a well-sheltered zone occurs a short distance downwind

* Where they run far from measurements, the contour positions are uncertain.

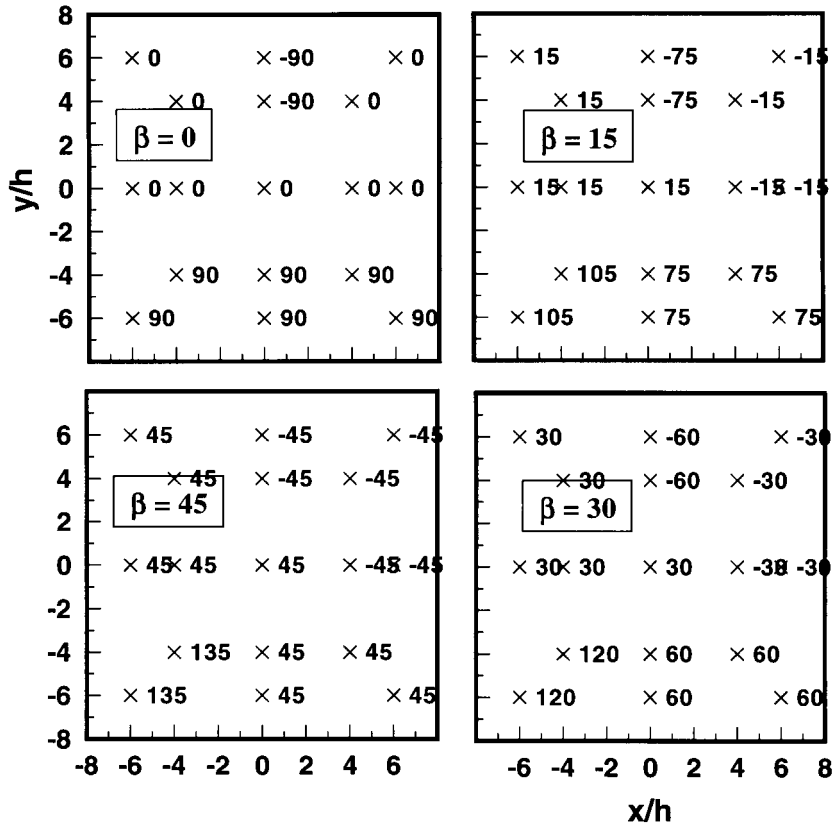

Figure 10. Showing the reduced wind direction β_r at instrumented plot locations for each of four absolute wind directions: Clockwise from top left, $\beta = (0°, 15°, 30°, 45°)$. At any of the given plot locations, measured mean wind reduction can be read off Figures 3 to 7 for each of the absolute wind directions, resulting in the contour patterns of Figures 11 to 14. The mean wind patterns for all other absolute wind directions (at 15° intervals) are implied (due to symmetry) by those given. (Note that these entries do not give the *actual* local reduced wind directions at the given points, which were generally not measured: these are transformations of the outside wind direction, taking into account the symmetry applying at the given point).

from the protecting fence, with relative windspeeds $U/U_0 \leq 0.4$; as would also occur downwind of an isolated fence, and as has already been seen from Figure 9, cup windspeed increases further downwind towards the leeward region of the plot. The most interesting aspect of these contour plots is that as β increasingly deviates away from normal incidence $\beta = 0°$, one sees the progression into the plot of a distinct corner effect off the north-east corner (there are obvious extensions to other corners with other absolute wind directions, by symmetry), with the protected zone entirely missing along the downwind diagonal in the case $\beta = 45°$ ('corner flow'),

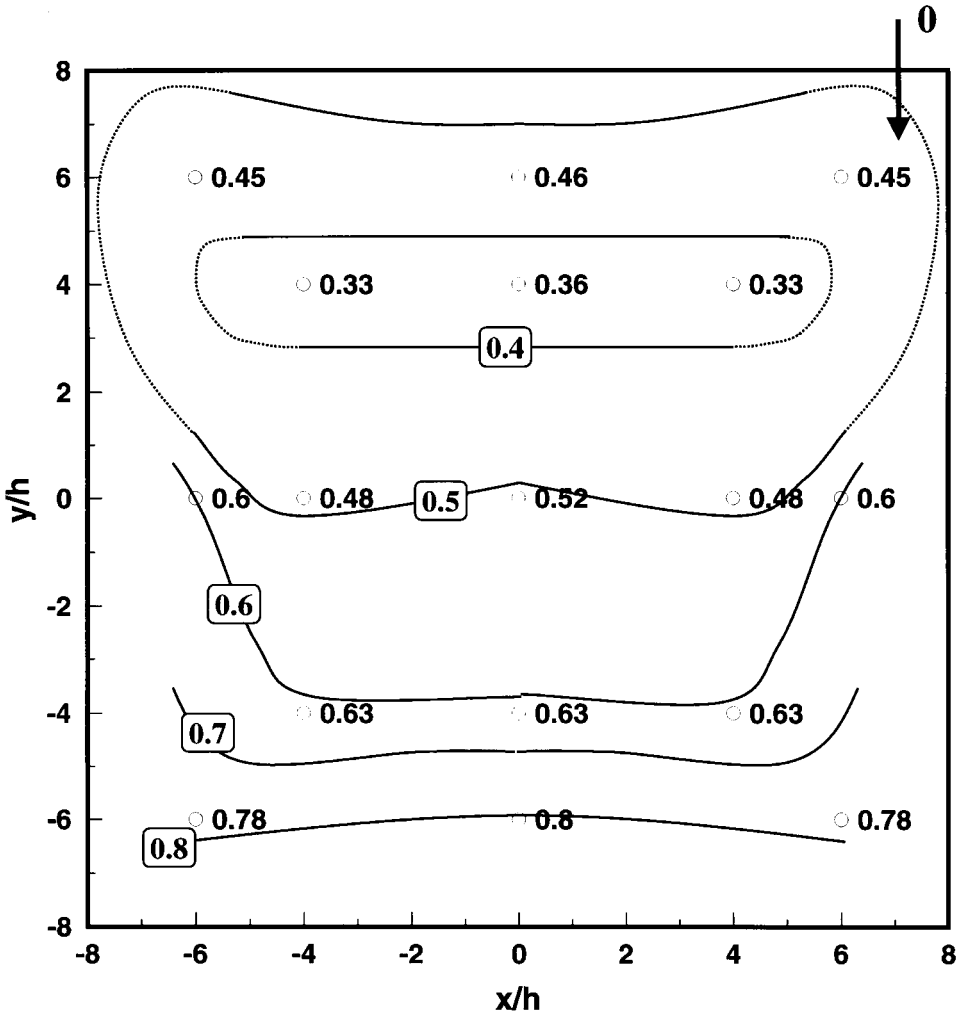

Figure 11. Hand-drawn contours (and point values off Figures 3 to 7) of relative cup windspeed U/U_0 in the plot at height $z/h = 0.5$, for an absolute wind direction $\beta = 0°$. Dashed extensions to the $U/U_0 = 0.4, 0.5$ contours are very tentative.

though with still a good level of shelter close behind the two (oblique) side-fences.* The core of strong winds caused by the corner is also quite important in the flow at $\beta = 30°$.

* Figure 14 may be compared with Richards' (1986) similar Figure 3 for an elongated *rectangular* windbreak.

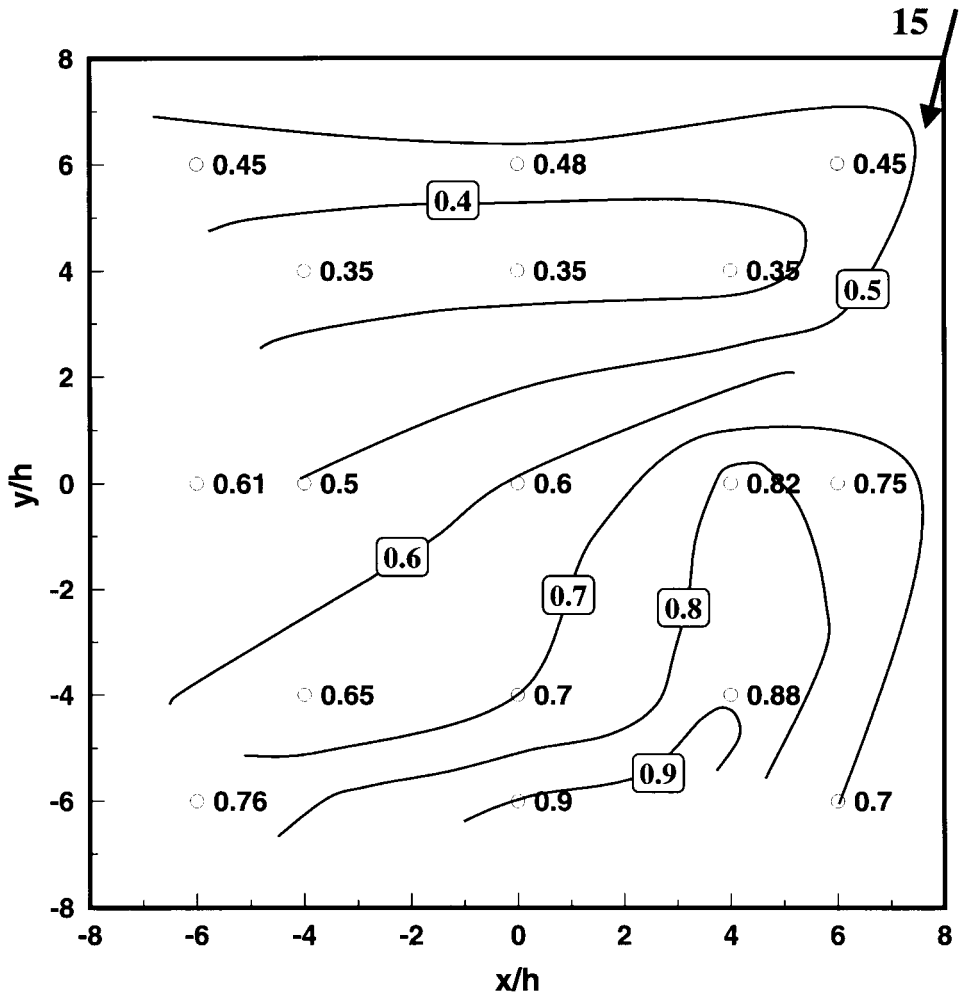

Figure 12. Hand-drawn contours (and point values off Figures 3 to 7) of relative cup windspeed U/U_0 in the plot at height $z/h = 0.5$, for an absolute wind direction $\beta = 15°$.

6. Other Velocity Statistics in the Plot

6.1. Mean vertical velocity

Given these strong disturbances to the mean horizontal windspeeds, one expects mean vertical velocities to be non-zero in the shelter. Figure 15a gives a computed streamwise profile of W along $z/H \approx 1$, from a numerical simulation of winds perpendicular to a long, isolated stretch of the present fence, and indicates a strong, narrow updraft peaking just upwind from the barrier (but with $W > 0$ almost to $x/h = 4$ downwind), and a broader, weaker downdraft in the lee.

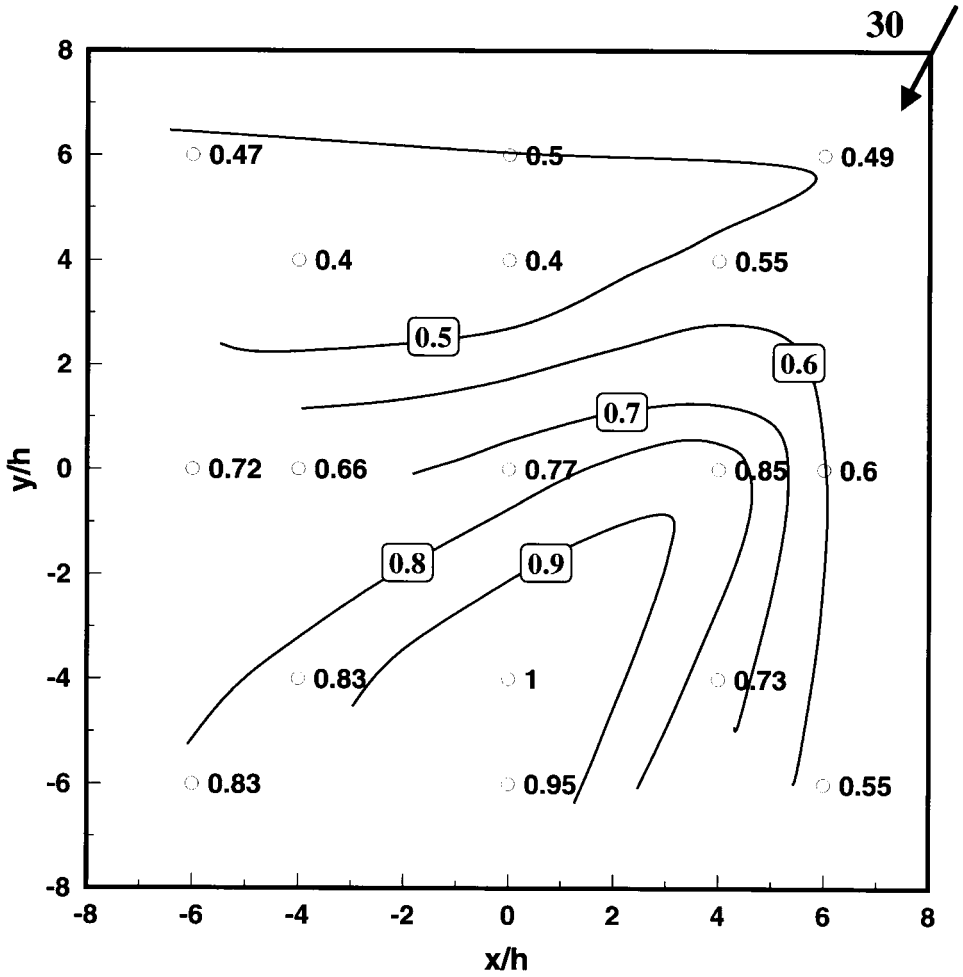

Figure 13. Hand-drawn contours (and point values off Figures 3 to 7) of relative cup windspeed U/U_0 in the plot at height $z/h = 0.5$, for an absolute wind direction $\beta = 30°$.

Figures 15b and 15c give observed mean vertical velocity W/u_{*0} at the corner position $2h$ from fences and at plot centre, versus reduced mean wind direction β_r. For both these positions, $\beta_r = 0°$ signifies a wind approaching the upwind fence at perpendicular incidence. These data stem from sonic measurements, and here (and throughout this section) the data selection criteria 'α' were supplemented by the requirement that the mean velocity be from the front of the in-plot sonic.

For perpendicular incidence ($\beta_r = 0^o$), the observed mean vertical velocities at both positions are comparable with those computed (Figure 15a) at corresponding distances ($x/h = 2, 8$) downwind from an isolated fence. But as $|\beta_r|$ increases (i.e., oblique incidence), a strong downdraft ($W/u_{*0} < -1$) forms close in to the corner (where, for perpendicular incidence, a weak updraft occurs), and the downdraft

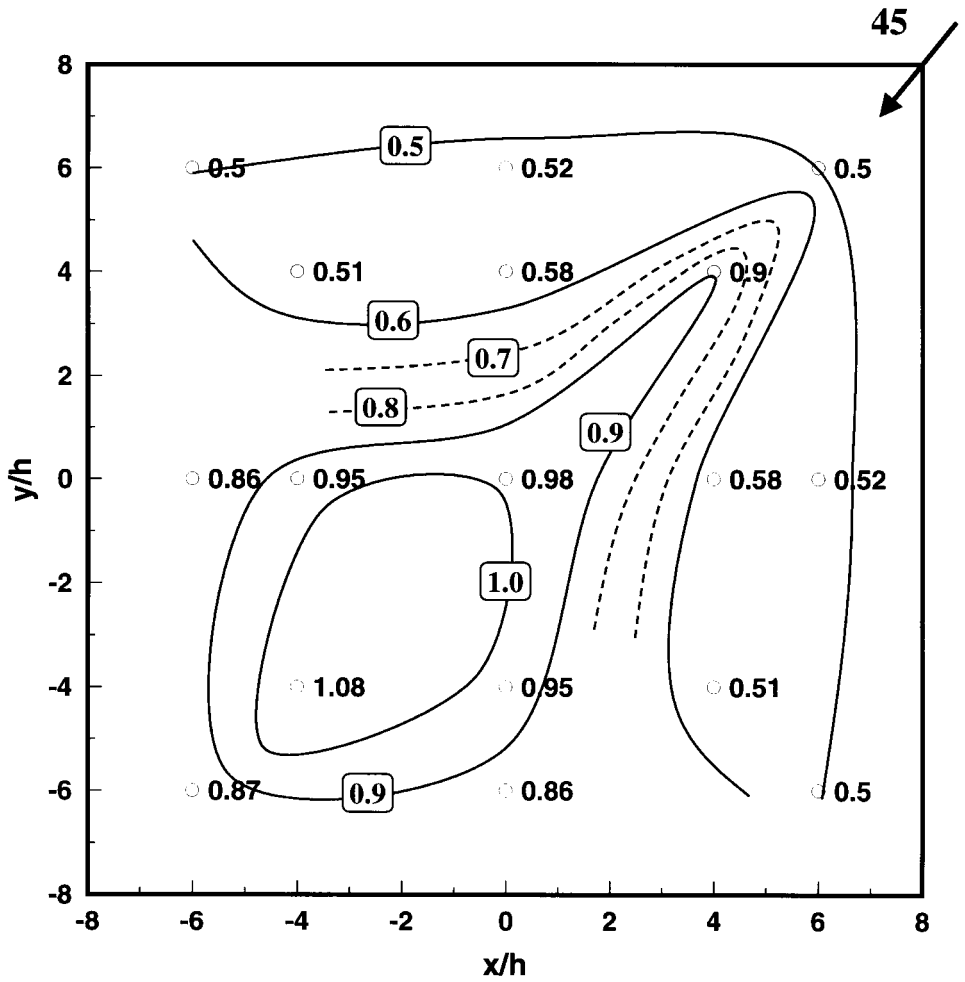

Figure 14. Hand-drawn contours (and point values off Figures 3 to 7) of relative cup windspeed U/U_0 in the plot at height $z/h = 0.5$, for an absolute wind direction $\beta = 45°$ (cf. Figure 3 of Richards, 1986).

at plot centre (present even for wind at perpendicular incidence) is accentuated. Data from plot centre indicate the vertical velocity is weaker at $z/h = 0.5$ than at $z/h = 0.8$; in view of the no-leak condition ($\mathrm{Lim}_{z\to 0}\ W = 0$), this is to be expected.

That there should be a considerable degree of scatter in these measurements of a small W is also unsurprising. The in-plot CSAT3 sonic was re-oriented several times, and each time re-levelled according to the built-in bubble-level, which could not have been accurate to better than about $\pm 1°$. Levelling errors would not be negligible relative to the streamline inclination associated with the vertical motion (for example, with $W/u_{*0} \approx 0.2$ and assuming $u_{*0} \approx 0.2$ m s^{-1} and $U \approx 2$ m s^{-1},

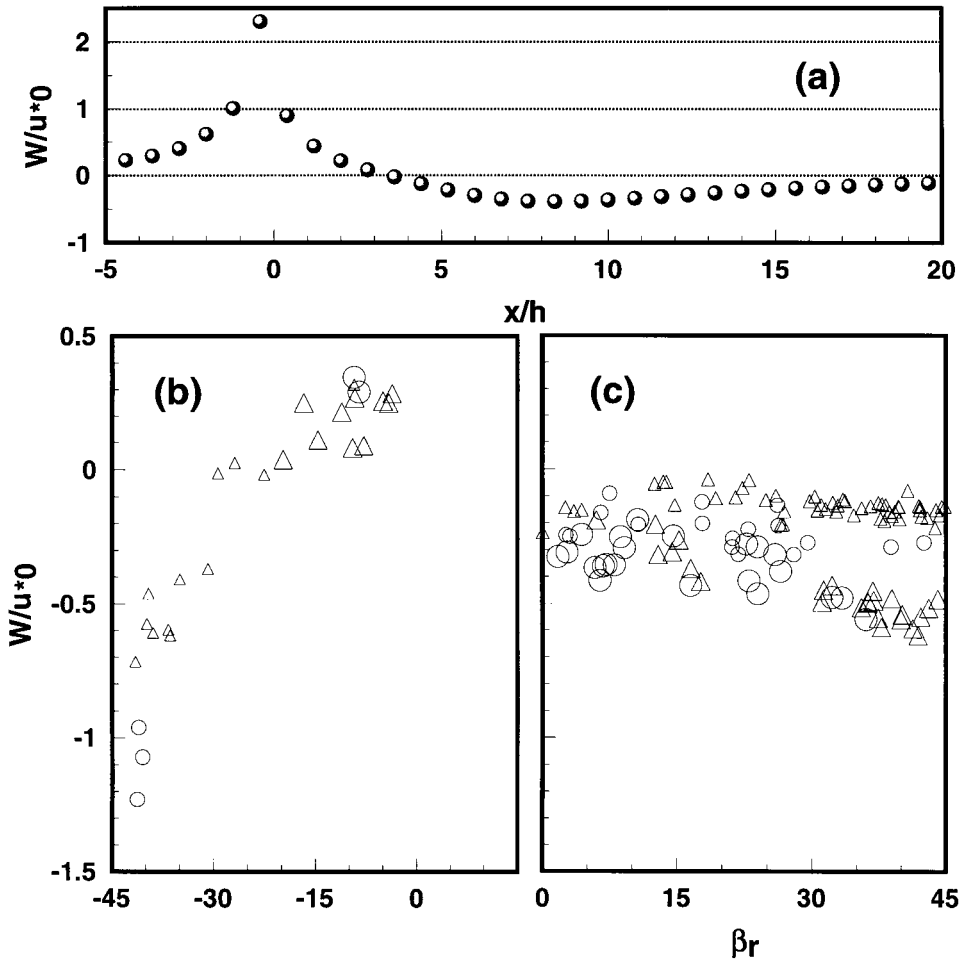

Figure 15. Mean vertical velocity: (a) Streamwise profile along $z/h = 1$, according to numerical simulation of neutrally-stratified flow perpendicular to an infinite fence ($k_{r0} = 2.4$, $h = 1.25$ m, $z_0 = 0.015$ m); (b) observed in corner of square plot $2h$ from fences at $z/h = 0.8$ (smaller symbols do not satisfy $160° \leq \beta \leq 330°$); and (c) observed at plot centre at $z/h = 0.8$ (large symbols) and $z/h = 0.5$ (small symbols): ○, Stable stratification; △, unstable stratification.

plot centre streamline inclination $\text{atan}(W/U) \approx 2°$). Furthermore for fixed β_r, a *fixed* sonic levelling error would introduce *different* apparent W, according to the *true* mean wind direction that has 'produced' β_r; that is, the symmetry assumed in reducing true wind direction to β_r is invalidated by sonic levelling error (e.g., a perfect 'corner flow' relative to plot centre occurs for each of the absolute wind directions $\beta = (45°, 135°, 225°, 315°)$, although the selection criteria reject the first two cases, i.e., easterlies). In the region $5° \leq \beta_r \leq 10°$ on Figure 15c, data are contributed from west–north–west, west–south–west, south–south–west and

south–south–east, likely (in conjunction with imperfect levelling) explaining the scatter.

6.2. DIRECTIONAL DEVIATION

When the wind strikes an isolated fence at oblique incidence, complex changes in wind direction occur; through the barrier and in its very near wake, streamlines are 'refracted' towards the normal to the fence. Figure 16b shows that at the centre of the square plot, streamlines deviate *away from the normal*.* Symmetry prohibits, in principle, any deviation of mean wind direction at plot centre from the approaching wind direction, for the two extreme cases of (a) perpendicular winds ($\beta_r = 0°$), or (b) corner winds ($\beta_r = 45°$). However for intermediate approach-wind directions, mean (reduced) wind direction β_{rc} at plot centre is larger than β_r, which implies the streamlines have been refracted away from the normal to the fence upwind. Figure 16a shows the streamline refraction observed in the corner of the plot (limited observations with the sonic in that position did not allow to cover the full range in β_r). There is no refraction at $\beta_r = -45°$ (as expected by symmetry) and only weak refraction for perpendicular incidence ($\beta_r = 0°$; no refraction, for a long isolated fence). For other approach angles, streamlines in the corner again deviate *away* from the normal to the upwind fence.

6.3. TURBULENCE

As noted earlier, an isolated windbreak generates a zone of enhanced turbulence spreading downwind from its upper edge, while underneath that zone, turbulence is reduced. At the centre of the present plot, distance $8h$ from the fence (when $\beta_r = 0°$), one would expect to be at the outer margin of the quiet zone, or in the turbulent zone. Wilson (1987) observed σ_w^2 to be increased by factors of ($\approx 2, \approx 2.5$) at heights $z/h = (0.5, 1)$, at downwind distance $x/h = 8$ from an isolated fence (porosity 50%).

Figure 17 gives normalized observations of the standard deviation σ_w of vertical velocity and of $\sigma_{uv} = \sqrt{\sigma_u^2 + \sigma_v^2}$ (indicating 'horizontal turbulence') at plot centre.** Vertical turbulence (σ_w) is enhanced at plot centre relative to the reference point, by about $20 - 40\%$ at $z/h = 0.5$ and by up to 80% at $z/h = 0.8$; dependence of σ_w on β_r is weak at the lower level, but definite at $z/h = 0.8$. Argete and Wilson (1989) also observed this enhancement of σ_w at the centre of the plot (same fence; same D/H; but observed at a lower height, $z/h = 0.25$, and without selection as regards wind direction β_r), by up to about 40%, and with the suggestion of a relationship with $h/(-L)$ such that there is maximal increase

* The outlier at $\beta_r = 27°$ stems from a run during very unstable stratification, $L \approx -10$ m, during which the tower sonic reported $\sigma_v/u_* = 7.1$, $\sigma_\beta (\approx \sigma_v/U_s) \approx 34°$.

** Normalized on corresponding values at $z = 2$ m on the tower. Statistics from plot sonic are *not* subjected to rotation.

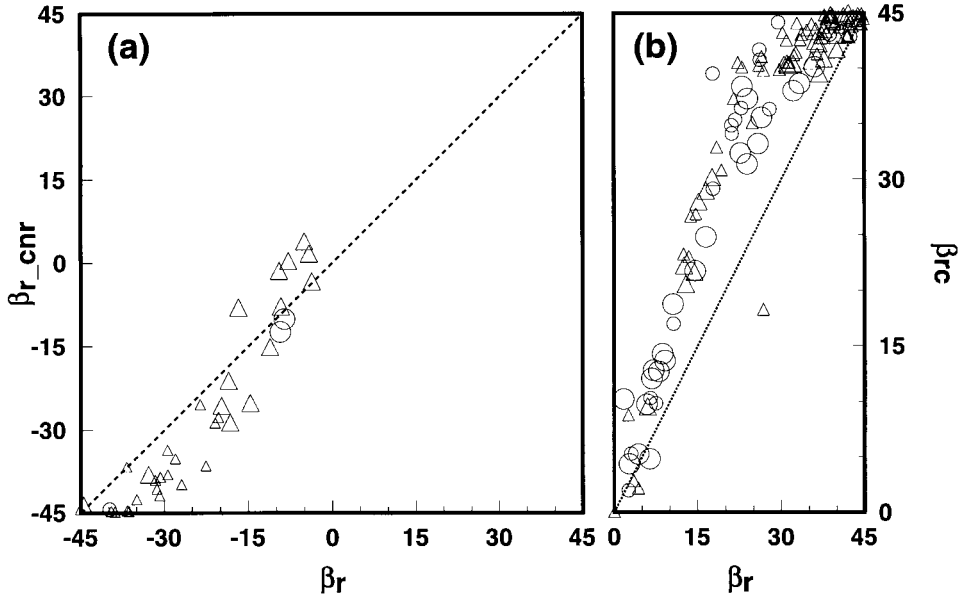

Figure 16. 'Streamline refraction': Reduced mean wind direction (a) in the corner position $2h$ from fences ($z/h = 0.8$; smaller symbols do not satisfy $160° \leq \beta \leq 330°$); and (b) at plot centre ($z/h = 0.8$, larger symbols; $z/h = 0.5$, smaller symbols; all data satisfy $160° \leq \beta \leq 330°$). ○, Stable stratification; △, unstable stratification.

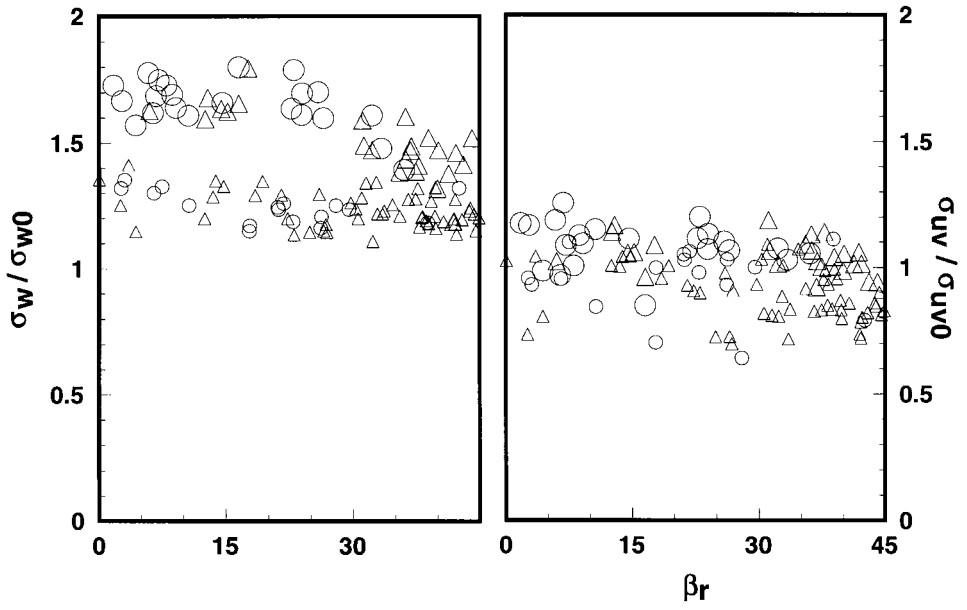

Figure 17. Ratios of σ_w and $\sigma_{uv} = \sqrt{\sigma_u^2 + \sigma_v^2}$ at centre of plot to their respective reference values in the open (small symbols, $z/h = 0.5$; large symbols, $z/h = 0.8$). ○, Stable stratification; △, unstable stratification. Observations satisfy $160° \leq \beta \leq 330°$.

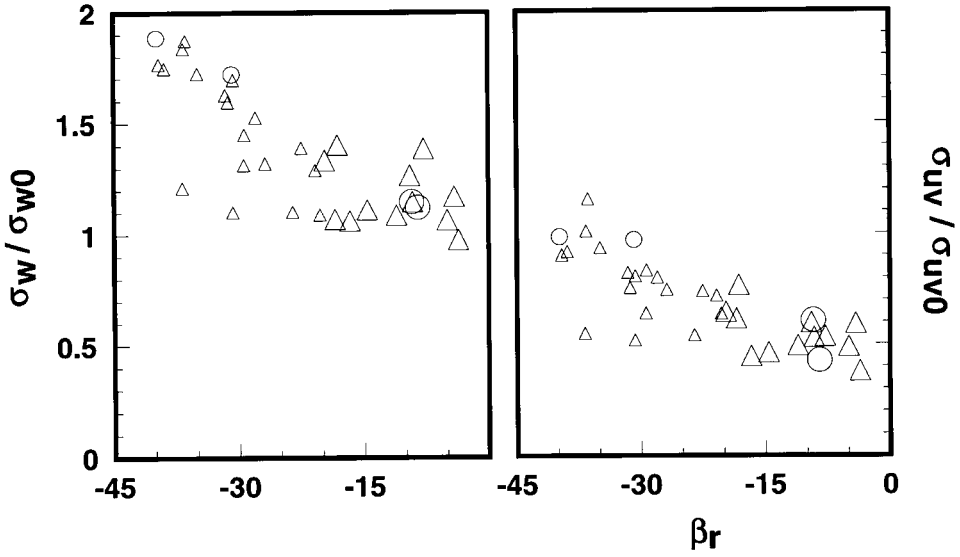

Figure 18. Ratios of σ_w and $\sigma_{uv} = \sqrt{\sigma_u^2 + \sigma_v^2}$ in corner of plot ($z/h = 0.8$, distance $2h$ from fences) to their respective reference values in the open. ○, Stable stratification; △, unstable stratification. Larger symbols are observations with absolute wind direction in the range $160° \leq \beta \leq 330°$; smaller symbols lie outside this range, but satisfy $135° \leq \beta \leq 350°$.

in σ_w for moderate instability (extreme instability is associated with weak winds, under which circumstances the windbreak will have minimal effect). The present observations do not suggest any definite relationship with stability. Interestingly, at plot centre σ_w tends to be *smaller* during corner flow ($\beta_r \approx 45°$) than for $\beta_r = 0$; this suggests that whatever 'structure' is induced during corner flow, when it is seen by an anemometer at plot centre, it manifests as a *less* turbulent wind. Horizontal windspeed fluctuations (characterized by σ_{uv}) at plot centre are slightly *reduced* at $z/h = 0.5$, but enhanced , though not nearly so much as is σ_w, at the higher elevation $z/h = 0.8$. Dependency of σ_{uv} on wind direction is weak.

Turning now to observations in a corner of the plot, Figure 18 indicates that provided the wind does not blow over a corner, the intensity of fluctuations in horizontal velocity is attenuated in the corner of the plot. However for corner flow, σ_w is enhanced in the immediate wake, and there is little if any protection in terms of horizontal velocity fluctuations. Thus corner flow enhances the level of turbulent kinetic energy (TKE) in the near wake of the fences, erasing the 'quiet zone' one observes behind a straight fence, or in the present configuration when $\beta_r \approx 0°$.

7. Conclusions

The wind direction 'signal' seen in these measurements is unambiguous and repeatable, only slightly sensitive to stratification and averaging interval, and though quite

complex, certainly plausible. Material and aerodynamic properties of the shelter, as well as the key micrometeorological variables, are prescribed. Therefore these disturbed wind data may usefully serve as a criterion for the credibility of micrometeorological wind models, both of RANS and LES class.* Do RANS models, for instance, produce the observed sensitivity of relative windspeed in the shelter to the external wind direction? An essential precursor to modelling studies will be to determine an appropriate *representation* of the fence-flow interaction, for oblique and cornered shelter-fences: we explore this topic in Appendix A.

Turning to the practical perspective, what is the utility of a windbreak of square configuration? We have seen that if the wind blows (nearly) perpendicularly over a side, mean wind speed is reduced below 50% of its value in the open ($U/U_0 \leq 0.5$) over about half the plot, and $U/U_0 \leq 0.9$ over the entire plot: the shelter is effective. But when the wind blows over a corner, 50% wind reduction is attained only over a fraction (about $\frac{1}{8}$ to $\frac{1}{5}$) of the plot, and $U/U_0 > 0.9$ over about ($\frac{1}{3}$ to $\frac{1}{2}$) of the plot area. Summarizing, and as a rough guideline, one may say that irrespective of atmospheric stratification, a 'small' ($1 \ll D/h \ll 100$) square or rectangular windbreak (a) offers little or no protection for points that lie broadly downwind from any of its four corners, excepting the small area that is wedged in very close ($\lesssim 2h$) to the corner, and (b) offers good protection for points lying (not too far) downwind of any side-fence that is roughly perpendicular to the mean wind (about the same level of protection as would be expected if the upwind fence were infinitely long, straight, and acting alone).

From a field study of winds in an array of *parallel* fences, McAneney and Judd (1991) concluded that 'In a practical sense, the data clearly demonstrate the difficulty of simultaneously reducing both mean windspeeds and turbulence at crop levels using repeated windbreaks at conventional horticultural spacings'. The data given here demonstrate that intersections further complicate the aerodynamics, and compromise the utility, of windbreak networks.

Acknowledgements

This work has been supported by research grants from the Natural Sciences and Engineering Research Council of Canada (NSERC) and the Canadian Foundation for Climate and Atmospheric Sciences (CFCAS).

* Equally, this would be an interesting test flow for the 'discrete vortex method', now being applied to three-dimensional flows with large Reynolds number (e.g., www.vorcat.com).

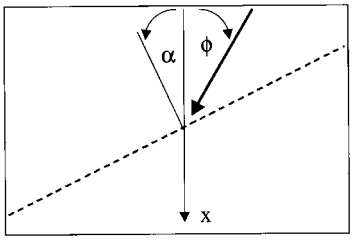

Figure A1. Mean wind vector upwind from a porous barrier inclined obliquely (angle α) relative to the x-axis, which coincides with the wind direction well upstream. The pressure drop across the barrier is determined by the projection of the wind vector onto the normal to the barrier, and the resistance coefficient k_{r0}.

Appendix A: Computational Representation of an Obliquely-Oriented Windbreak

Let the x-axis lie along the mean wind direction far upstream of the barrier. The Reynolds-averaged (three-dimensional) $\overline{u}$-momentum equation is:

$$\frac{\partial}{\partial x}\left(\overline{u}^2 + \overline{u'^2} + \overline{p}\right) + \frac{\partial}{\partial y}\left(\overline{u}\,\overline{v} + \overline{u'v'}\right) + \frac{\partial}{\partial z}\left(\overline{u}\,\overline{w} + \overline{u'w'}\right) = S_u. \tag{A1}$$

The definition of the momentum sink S_u is more complex than in the case of a mean wind perpendicular to the barrier, due to the deviation of the wind from the approach path (Figure 19). In the convention shown, the deflection angle ϕ will have the same sign as the obliquity angle α (recall the observation of Mulhearn and Bradley (1977): 'Upwind of the fence, the air close to the ground is deflected along the shelterbelt.'). Close to the fence the wind will turn back towards the normal to the barrier, forming the 'bleed flow' (this deviation is not shown on Figure A1).

The effective momentum sink S_u in Equation (A1) is most naturally specified with reference to a velocity 'at' the fence, but 'at' is not to be interpreted as meaning within the region where the wind deviates into the pores. It is consistent with Equation (1) to assume that the pressure drop across the barrier will be:

$$p_1 - p_2 = k_{r0}\,\rho\,V_\perp{}^2, \tag{A2}$$

where the component of mean velocity perpendicular to the fence

$$V_\perp = \sqrt{\overline{u}^2 + \overline{v}^2}\,\cos(\alpha + \phi) \tag{A3}$$

(here we neglect the influence of the mean vertical velocity, and more importantly, the differing orientation of the bleed flow). Now, as we are interested in the x-component of the implied pressure gradient force, i.e., the projection onto the

x-axis of the reaction of the fence against the flow, the momentum sink for an infinitely long fence passing through the origin ($x = y = 0$) is

$$S_u = k_{r0}\left(\overline{u}^2 + \overline{v}^2\right)\cos^2(\alpha+\phi)\cos(\alpha)\,\delta\left[y\sin(\alpha) - x\cos(\alpha)\right]s(z-h), \quad \text{(A4)}$$

where the localizing δ-function could be adjusted (or replaced) so as to specify other locations (or configurations; e.g., curves; corners) of the fence. The corresponding sink in the $\overline{v}$-momentum equation is

$$S_v = k_{r0}\left(\overline{u}^2 + \overline{v}^2\right)\cos^2(\alpha+\phi)\sin(\alpha)\,\delta\left[y\sin(\alpha) - x\cos(\alpha)\right]s(z-h). \quad \text{(A5)}$$

From Equations (A4) and (A5), which are heuristic, we may anticipate that wind protection in the lee of an obliquely-oriented fence will be less effective than behind a normally-oriented fence (for which case $\alpha = \phi = 0$, and the delta function reduces to $\delta(x-0)$). The deflection angle $\phi = \text{atan}(\overline{v}/\overline{u})$ is not independent of α, and being a function of the mean velocity field, is determined non-locally as the solution of Equation (A1) and its companion equations. For small obliquity angle, $|\alpha| \approx 0$, it may appear that $S_u \propto \cos^3(\alpha)$, but such an inference would neglect adjustments in $\overline{u}$, $\overline{v}$ concomitant with the variation in α (for a fixed approach flow, i.e., we consider α alone to vary as an 'external parameter', with fixed far-upstream conditions).

But Equations (A4) and (A5) cannot be the whole story, for consider the case that the fence is *parallel* to the approach flow, i.e., $\alpha = 90°$. By symmetry, there can be no deflection, so $\overline{v} = \phi = 0$. The delta function reduces to $\delta(y-0)$, correctly locating a momentum sink along the (infinitely-long) fence, but a sink of *zero-strength* – which of course has no effect. In reality, mean streamwise velocity (at the fence), under this condition, would probably be small, as if to say a no-slip condition should be applied (though this would not be true near the upwind end of a *finite* fence in a parallel-approach wind).

Then what have we neglected in Equations (A4) and (A5)? We have (of necessity) overlooked momentum transfer to the barrier by the small-scale, unresolved mean pressure gradients in the very near vicinity of our rough, porous fence-surface (unresolved pressure drag), and less importantly viscous drag. The influence of these processes can be neglected (relative to the drag we resolve via Equation (A4)) only provided the mean wind direction is not too close to being parallel to the fence. In reality, their action is to ensure that $\overline{u} \approx 0$ along the fence (in the condition that the fence is *parallel* to the mean wind), with a zone of reduced mean wind $\overline{u}$ on either side, i.e., a lateral wind shear ($\partial\overline{u}/\partial y$) zone that is bound to result in a transfer of $\overline{u}$-momentum to the fence* (that is, a drag) by virtue of the Reynolds stress $\partial\overline{u'v'}/\partial y$ appearing in Equation (A1). In this condition of a mean wind parallel to a porous barrier, there would also be, in reality, strong damping of the perpendicular

* When one holds, for example, a porous plate *parallel* to the the wind, the force required to support it is far smaller than when it is held *against* the wind: But it is not zero!

velocity *fluctuations* v' through the fence, i.e., $\overline{v'^2}$ would be reduced at the fence, and the term $\partial\overline{v'^2}/\partial y$ in the $\overline{v}$-equation would attain some importance (even though $\overline{v} = 0$ under the present condition that $\alpha = 0$, the $\overline{v}$ momentum equation remains a non-trivial member of the governing suite of coupled equations).

The objective in parametrizing the influence of a porous barrier as a momentum sink is to avoid the necessity to introduce additional conditions internal to the computational domain – to avoid the complication that this is really a multiply-connected flow domain with a complex boundary. Thus, one may need to adjust or supplement the sinks (S_u, S_v) so that, even along a finite length of wind-parallel fence, a retarding influence is felt, becoming (effectively) equivalent to a no-slip condition, if the fence stretches far alongwind. One means to introduce that wanted effect might be to replace the projection factors $\cos(\alpha)$, $\sin(\alpha)$ appearing respectively in S_u, S_v by something like:

$$\cos(\alpha) \leftarrow d_0 + (1 - d_0)\cos(\alpha), \tag{A6a}$$

$$\sin(\alpha) \leftarrow d_0 + (1 - d_0)\sin(\alpha), \tag{A6b}$$

where d_0, the parallel drag correction factor, satisfies $0 < d_0 \ll 1$. Alternatively though, it may be that the normal stress gradients across the fence, constituting a disturbance in the momentum equations, and assured by a careful representation of TKE sinks at the fence, would give rise naturally to the expected mean drag in parallel flow. Numerical simulations might determine this, although ambiguity as to the proper treatment of the RANS equation for the TKE dissipation rate ϵ would arise.

References

Argete, J. C. and Wilson, J. D.: 1989, 'The Microclimate in the Centre of Small Square Sheltered Plots', *Agric. For. Meteorol.* **48**, 185–199.

Bradley, E. F. and Mulhearn, P. J.: 1983, 'Development of Velocity and Shear Stress Distributions in the Wake of a Porous Shelter Fence', *J. Wind Eng. Indust. Aerodyn.* **15**, 145–156.

Dyer, A. J. and Bradley, E. F.: 1982, 'An Alternative Analysis of Flux-Gradient Relationships at the 1976 ITCE', *Boundary-Layer Meteorol.* **22**, 3–19.

Heisler, G. M. and Dewalle, D. R.: 1988, 'Effects of Windbreak Structure on Wind Flow', *Agric. Ecosyst. Environ.* **22/23**, 41–69.

Jacobs, A. F. G. and Wartena, L.: 1987, 'Flow and Turbulence around Thin Fences in Perpendicular and Oblique Flow Direction', *Neth. J. Agric. Sci.* **35**, 7–20.

Judd, M. J., Raupach, M. R., and Finnigan, J. J.: 1996, 'A Wind Tunnel Study of Turbulent Flow around a Single and Multiple Windbreaks; Part 1: Velocity Fields', *Boundary-Layer Meteorol.* **80**, 127–165.

Kaimal, J. C. and Finnigan, J. J.: 1994, *Atmospheric Boundary Layer Flows*, Oxford University Press, 289 pp.

Koo, J.-K. and James, D. F.: 1973, 'Fluid Flow around and through a Screen', *J. Fluid Mech.* **60**, 513–538.

Laws, E. M. and Livesey, J. L.: 1978, 'Flow through Screens', *Annu. Rev. Fluid Mech.* **10**, 247–266.
McAneney, K. J. and Judd, M. J.: 1991, 'Multiple Windbreaks: An Aeolean Ensemble', *Boundary-Layer Meteorol.* **54**, 129–146.
McNaughton, K. G.: 1988, 'Effects of Windbreaks on Turbulent Transport and Microclimate', *Agric. Ecosyst. Environ.* **22/23**, 17–39.
McNaughton, K. G.: 1989, 'Micrometeorology of Shelterbelts and Forest Edges', *Phil. Trans. Roy. Soc. Lond. Ser. B* **324**, 351–368.
Mulhearn, P. J. and Bradley, E. F.: 1977, 'Secondary Flows in the Lee of Porous Shelterbelts', *Boundary-Layer Meteorol.* **12**, 75–92.
Papadopoulos, K. H., Stefanatos, N. C., Paulsen, U. S., and Morfiadakis, E.: 2001, 'Effects of Turbulence and Flow Inclination on the Performance of Cup Anemometers in the Field', *Boundary-Layer Meteorol.* **101**, 77–107,
Raine, J. K. and Stevenson, D. C.: 1977, 'Wind Protection by Model Fences in a Simulated Atmospheric Boundary Layer', *J. Ind. Aerodynam.* **2**, 159–180.
Rao, K. S., and Wyngaard, J. C., and Cote, O. R.: 1974a, 'Local Advection of Momentum, Heat, and Moisture in Micrometeorology', *Boundary-Layer Meteorol.* **7**, 331–348.
Rao, K. S. and Wyngaard, J. C., and Cote, O. R.: 1974b, 'The Structure of the Two-Dimensional Internal Boundary Layer over a Sudden Change of Surface Roughness', *J. Atmos. Sci.* **31**, 738–746.
Richards, P. J.: 1986, 'Wind Protection in the Vicinity of Right Angle Wind Break Corners', in *Proceedings of the 9th Australasian Fluid Mechanics Conference*, Auckland, December 1986, pp. 193–195.
Richards, P. J., Kay, E. F., Russell, D., and Wilson, G. R. C.: 1984, 'Porous Artificial Windbreaks in Oblique Winds'. Paper 67/84, Institute of Professional Engineers of New Zealand (IPENZ), Conference, Hastings, February 1984.
Seginer, I.: 1975, 'Flow around a Windbreak in Oblique Wind', *Boundary-Layer Meteorol.* **9**, 133–141.
Wang, H. and Takle, E. S.: 1995, 'A Numerical Simulation of Boundary-Layer Flows near Shelterbelts', *Boundary-Layer Meteorol.* **75**, 141–173.
Wang, H. and Takle, E. S.: 1996, 'On Shelter Efficiency of Shelterbelts in Oblique Winds', *Agric. For. Meteorol.* **81**, 95–117.
Wang, H. and Takle, E. S.: 1997, 'Model-Simulated Influences of Shelterbelt Shape on Wind-Sheltering Efficiency', *J. Appl. Meteorol.* **36**, 695–704.
Webb, E. K.: 1970, 'Profile Relationships: The Log-Linear Range and Extension to Strong Stability', *Quart. J. Roy. Meteorol. Soc.* **96**, 67–90.
Wilson, J. D.: 1985, 'Numerical Studies of Flow through a Windbreak', *J. Wind Eng. Ind. Aerod.* **21**, 119–154.
Wilson, J. D.: 1987, 'On the Choice of a Windbreak Porosity Profile', *Boundary-Layer Meteorol.* **38**, 37–49.
Wilson, J. D.: 1988, 'A Second-Order Closure Model for Flow through Vegetation', *Boundary-Layer Meteorol.* **42**, 371–392.
Wilson, J. D.: 1997, 'A Field Study of the Mean Pressure about a Windbreak', *Boundary-Layer Meteorol.* **85**, 327–358.
Wilson, J. D. and Yee, E.: 2003, 'Calculation of Winds Disturbed by an Array of Fences', *Agric. For. Meteorol.* **115**, 31–50.
Wilson, J. D., Flesch, T. K., and Harper, L. A.: 2001, 'Micro-Meteorological Methods for Estimating Surface Exchange with a Disturbed Windflow', *Agric. For. Meteorol.* **107**, 207–225.
Wilson, J. D., Swaters, G. E., and Ustina, F.: 1990, 'A Perturbation Analysis of Turbulent Flow through a Porous Barrier', *Quart. J. Roy. Meteorol. Soc.* **116**, 989–1004.